Atmos. Meas. Tech. Discuss., doi:10.5194/amt-2016-148, 2016
Manuscript under review for journal Atmos. Meas. Tech.
Published: 30 May 2016

Atmospheric Measurement Techniques
Open Access
Discussions

Absolute calibration of the colour index and O_4 absorption derived from Multi-AXis (MAX-) DOAS measurements and their application to a standardised cloud classification algorithm

Thomas Wagner, Steffen Beirle, Julia Remmers, Reza Shaiganfar, Yang Wang

Max-Planck-Institute for Chemistry, Mainz, Germany

Correspondence to: Thomas Wagner (thomas.wagner@mpic.de)

Abstract. A method is developed for the calibration of the colour index (CI) and the O_4 absorption derived from Differential Optical Absorption Spectroscopy (DOAS) measurements of scattered sunlight. The method is based on the comparison of measurements and radiative transfer simulations for well-defined atmospheric conditions and viewing geometries. Calibrated measurements of the CI and the O_4 absorption are important for the detection and classification of clouds from MAX-DOAS observations. Such information is needed for the identification and correction of the cloud influence on Multi-AXis (MAX-) DOAS profile inversion results, but might be also be of interest on their own, e.g. for meteorological applications. The calibration algorithm was successfully applied to measurements at two locations: Cabauw in the Netherlands and Wuxi in China. We used CI and O_4 observations calibrated by the new method as input to our recently developed cloud classification scheme and adapted also the corresponding threshold values accordingly. For the observations at Cabauw good agreement is found with the results of the original algorithm. Together with the calibration procedure of the CI and O_4 absorption the cloud classification scheme, which was tuned to specific locations/conditions so far, can now be applied consistently to MAX-DOAS measurements at different locations. In addition to the new threshold values, further improvements were introduced to the cloud classification algorithm, namely a better description of the SZA dependence of the threshold values and a new set of wavelengths for the determination of the CI. We also indicate specific areas for future research to further improve the cloud classification scheme.

1 Introduction

Multi-AXis-Differential Optical Absorption Spectroscopy (MAX-DOAS) measurements are a widely used remote sensing technique for the measurement of atmospheric trace gases and aerosols (e.g. Hönninger and Platt, 2002; Wittrock et al., 2004; Heckel et al., 2005; Frieß et al., 2006; Irie et al., 2008; Clémer et al., 2010; Li et al., 2010; Wagner et al., 2011, Ma et al., 2013, Wang et al., 2014, Hendrick et al., 2014, Wang et al., 2015, Vlemmix et al., 2015). MAX-DOAS measurements can be strongly affected by clouds (Wagner et al., 2004, 2011, 2014; Gielen et al., 2014; Wang et al., 2015). Thus cloud contaminated measurements have to be flagged, excluded from further processing, or corrected for the effects of clouds. Different algorithms for the identification and classification of clouds based on MAX-DOAS measurements have recently been developed. They are based on several quantities derived from the measured spectra (Wagner et al., 2014; Gielen et al., 2014; Wang et al., 2015). These quantities include:

a) A so called colour index (CI, see e.g. Sarkissian et al., 1991, 1994), which is defined as intensity ratio for two selected wavelengths. In this study we define the CI as a ratio of the intensity at the shorter wavelength to the intensity at the longer wavelength:

$$\mathrm{CI} = \frac{I_{short}}{I_{long}} \qquad (1)$$

b) The measured radiance at a selected wavelength. Here it should be noted that usually (MAX-) DOAS instruments are not radiometrically calibrated. Thus we use the term 'radiance' here in a broader sense also for the measured signal, e.g. expressed as counts per second.

c) The absorption of the oxygen dimer O_4 (Greenblatt et al., 1990).

d) The strength of the so called Ring effect (the filling-in of solar Fraunhofer lines by rotational Raman scattering, see Grainger and Ring, 1961, Wagner et al., 2014).

It was shown by Gielen et al. (2014) and Wagner et al. (2014) that the CI is very sensitive to the presence of clouds. It is thus well suited for their detection, especially because for zenith observations clouds always lead to a decrease of the CI compared to clear sky conditions (if the CI is defined with the intensity at the shorter wavelength divided by the intensity at the longer wavelength). In contrast, the other quantities mentioned above can be both increased or decreased in the presence of clouds depending on the cloud properties, wavelength and viewing geometry. Because of the unique dependence of the CI on the occurrence of clouds, the CI is usually used as primary quantity for the detection of clouds. From the other quantities, especially from the radiance and the absorption of the oxygen dimer O_4 important additional information on cloud properties can be derived (e.g. on the presence of optically thick clouds or fog, see Wagner et al., 2014, Gielen et al., 2014; Wang et al., 2015). Since Ring effect measurements do not provide significant extra information, and because the quantitative analysis of the Ring effect is rather complicated, the Ring effect is not further considered here.

The identification and classification of clouds is usually based on the comparison of the measured quantities to thresholds. These threshold values can e.g. be derived from measurements at clear days. Another, more universal method is the determination of the threshold values from radiative transfer simulations. However, since MAX-DOAS instruments are usually not radiometrically calibrated, a direct quantitative comparison of measured and simulated quantities is not possible, which hampers the direct application of threshold values derived from radiative transfer simulations. To overcome this limitation, in this study we develop calibration procedures for the CI and the O_4 absorption and apply them to MAX-DOAS observations.

The proposed CI calibration comprises the determination of a proportionality constant, which converts the measured values into well-defined quantities (i.e. radiance ratios for the selected wavelengths). Similar suggestions for the calibration of the CI were already presented by Gielen et al. (2014) and Wagner et al. (2014).

For the O_4 measurements the calibration comprises the determination and correction of an additional offset (the O_4 absorption of the Fraunhofer reference spectrum, FRS). A similar calibration could be applied to the Ring effect observations, but Ring effect observations are not considered here. We also do not apply a calibration of the measured radiances (e.g. Wagner et al., 2015) because of the considerably larger effort of such a calibration

Atmos. Meas. Tech. Discuss., doi:10.5194/amt-2016-148, 2016
Manuscript under review for journal Atmos. Meas. Tech.
Published: 30 May 2016

Atmospheric Measurement Techniques Discussions
Open Access

compared to the calibration of the CI and the O_4 absorption. Here it should be noted that in previous studies (Wagner et al., 2014; Wang et al., 2015) calibration procedures for the radiance were applied based on selected clear sky observations. But in these studies inconsistencies, especially for low SZA, were determined mainly caused by an imperfect knowledge and description of the aerosol optical properties. Moreover, the methods for the radiance calibration used in these studies are not (yet) applicable in a standardised way.

In addition to the application of the new threshold values, further improvements to the original classification scheme (Wagner et al., 2014) were introduced:

a) The determination of the threshold values is based on well-defined atmospheric scenarios.

b) The new thresholds better account for SZA dependencies.

c) A new set of wavelengths is used for the CI: The old wavelength pair (320 nm / 420 nm, see Wagner et al., 2014) is replaced by 330 nm / 390 nm. The new wavelength pair has several advantages: the new shorter wavelength (330nm) is less affected by the atmospheric ozone absorption than the original choice (320 nm). The new longer wavelength (390 nm) has the advantage that it is covered by typical UV MAX-DOAS instruments (while 440 nm is often not). For 390 nm also the variability of the surface albedo is smaller than for 440 nm.

Together with the new calibration procedures for the CI and the O_4 absorption, the updated threshold values constitute the basis for a universal cloud classification scheme for DOAS measurements of scattered sunlight.

The calibration procedures for the CI and the O_4 absorption are described in the first part of our paper (sections 2 and 3). In section 4, we apply both new calibrations to the measurements used for the development of the original cloud classification algorithm (Wagner et al., 2014), determine new threshold values and compare the results of the new and original algorithms.

In section 5 particular problems for MAX-DOAS measurements at low and high latitudes are discussed. Section 6 presents conclusions and outlook.

2 Calibration of the CI

DOAS instruments are usually not radiometrically calibrated. Thus measured radiances and CI derived from MAX-DOAS or zenith sky DOAS measurements cannot be directly compared to the results from radiative transfer simulations. But the CI derived from the measurements (CI_{meas}) can be converted to calibrated CI (CI_{cal}) by multiplication with a proportionality constant β:

$$\mathrm{CI}_{\mathrm{cal}} = \mathrm{CI}_{\mathrm{meas}} \cdot \beta \qquad (2)$$

β can be determined by comparison of measured and simulated CI under well-defined conditions (see e.g. Wagner et al., 2014 and Gielen et al., 2014; Wang et al., 2015). Wagner et al. (2014) used measurements during a clear morning with constant AOD (derived from a sun photometer) for the calibration of the CI, radiance, O_4 absorption, and Ring effect. Gielen et al. (2014) applied a more universal approach by considering CI values over extended periods of time. They compared cluster points for minima and maxima of the CI to results of radiative transfer simulations. In our study we basically follow their approach, but we also apply two important modifications:

a) We only consider the minimum CI. As shown by Gielen et al. (2014), the maximum CI varies strongly with changing AOD, especially for low AOD. Thus the comparison of measured and simulated maximum CI depends critically on the AOD during the considered period, which is usually unknown. In contrast, the minimum CI depends only slightly on the specific atmospheric properties and measurement conditions (for details see below).

b) We do not use static threshold values, but consider the SZA dependence (of the minimum CI).

We also propose to use the wavelength pair of 330 nm and 390 nm for the calculation of the CI (see the discussion in the introduction). In the following the original CI is indicated by CI_{orig} and the new CI by CI_{new}. In Fig. 1 simulation results for CI_{orig} and CI_{new} are shown for different aerosol and cloud conditions. For both CI two features are obvious:

a) As already shown by Gielen et al. (2014), the maximum CI depends strongly on the AOD. This finding confirms that the maximum CI is not well suited for the calibration of the CI.

b) Small CI are found for cloudy cases, but interestingly the minimum values do not always occur for the largest cloud optical depths. This finding is probably caused by multiple scattering inside the clouds, which also increases the probability of additional Rayleigh scattering. Depending on the chosen wavelengths and SZA, the minimum CI is found for cloud optical depths between 3 and 12 (but the CI for the different cloud optical depths varies only slightly). Here it should also be noted that the CI for cloudy conditions is almost independent on cloud height.

It should be noted that these simulations are performed not for an elevation angle of exactly 90°, but for 85°, because of the specific conditions of the measurements used here (Wagner et al., 2014). Thus the results differ slightly from those for exact zenith view (for more details see section 4.6). For the same reason, the simulation results in Fig. 1 are presented as function of time and not as a function of the SZA.

In Fig. 2 selected observations of CI_{orig} and CI_{new} during the Cabauw Intercomparison Campaign of Nitrogen Dioxide measuring Instruments (CINDI) campaign in Summer 2009 (Piters et al., 2012) are compared to simulation results (for aerosol-free conditions, low aerosol load and the minimum CI for cloudy conditions, see Fig. 1). Different y-axes are used for the measured (left) and simulated (right) CI. The maximum values of both axes were chosen according to the absolute radiance calibration for the respective wavelengths presented in Wagner et al. (2015). For CI_{orig} and CI_{new} most measurements fall into the area between the simulated minimum CI and those for an AOD of 0.1 (similar findings were presented by Gielen et al., 2014). Interestingly, several measurements falls slightly below the simulated minimum values. This finding, cannot be explained by the effect of measurement noise on the CI, which is very small (<<1% for the SZA range considered here). Instead, the low CI values are probably caused by 3D effects of broken clouds, which are not considered in our simulations. However, even the lowest measured CI are still close to the simulated minimum values indicating that the overall dependence of the CI is well represented by the model simulations (the detailed investigation of these 3D effects should be the topic of futures studies). The results in Fig. 2 indicate that the minimum CI obtained from measurements (or better an accumulation point, see below) over a period of several weeks are well suited for the calibration of the measured CI.

We propose a calibration procedure consisting of two steps:

First the measured CI are normalised (divided) by the corresponding simulated minimum CI (for the same SZA). The normalised CI for both wavelength pairs are shown in Fig. 3. The normalisation procedure mostly eliminates the SZA dependence of the measured minimum CI. However, for SZA > 60° (red vertical lines in Fig. 3), still a SZA

Atmos. Meas. Tech. Discuss., doi:10.5194/amt-2016-148, 2016
Manuscript under review for journal Atmos. Meas. Tech.
Published: 30 May 2016

Atmospheric Measurement Techniques Discussions

dependence is present. Thus only measurements with SZA < 60° are considered for the determination of the scaling factor.

In the next step, frequency distributions of the normalised CI values for SZA < 60° are calculated, see Fig. 4. Distinct accumulation points for the minimum CI for both wavelength pairs are obtained indicating the presence of clouds. Their maxima directly represent the (inverse of the) proportionality constant β (Eq. 2). Here it should be noted that for measurements at locations with low cloud probability a larger time period than for our method might be needed to achieve a sufficient number of cloudy measurements. The normalised CI of the accumulation point is determined by fitting a Gaussian curve to the frequency distribution after the cloud sky data were removed (data with normalised CI larger than 0.59 and 0.93 for the CI_{old} and CI_{new}, respectively. Note that the derived values are almost independent from the chosen clipping value. We also determined the uncertainty of the scaling factor from the Gaussian fit to <1%. In order to account for possible temporal variation of the instrument sensitivity, we applied the method separately to the measurements during the first and second half of the campaign and found deviations <2%. This value probably represents a more realistic uncertainty for the measurements used in our study. For CI_{orig} β is found to be 2.04 ± 0.04, and for CI_{new} 1.16 ± 0.02. The derived proportionality constants agree well with those calculated from the absolute radiance calibration presented in Wagner et al. (2015): 2.00 for CI_{orig} and 1.19 for CI_{new}.

In Fig. 4 also results for MAX-DOAS observations at Wuxi (China) for the new CI are shown (Wang et al., 2015). Measurements over a period from 1 January 2012 to 31 December 2012 were used. Like for the Cabauw measurements a clear peak is found indicating that the method works in a similar way for completely different locations and measurement conditions. The derived proportionality constant is different from that for the Cabauw measurements caused by the different (wavelength dependent) sensitivities of both instruments. Here it should be noted that differences of the aerosol properties at both locations could also contribute to the differences, but the effect of aerosols on the CI in the presence of clouds is typically below 2%.

3 Calibration of the O_4 absorption of the Fraunhofer reference spectrum

Also the O_4 calibration is performed by comparing the measurements to model simulations for specific atmospheric properties and measurement conditions. From the spectral analysis the O_4 slant column density (SCD) is derived, which represents the integrated O_4 concentration along the atmospheric light path. Since also the FRS contains atmospheric O_4 absorptions, the result of the spectral analysis eventually represents the difference of the O_4 SCDs of the measurement and the FRS, which is usually referred to as differential SCD or DSCD.

Both the O_4 SCD and DSCD can be converted to the corresponding O_4 AMF or O_4 DAMF:

$$AMF = SCD / VCD \quad (3)$$

$$DAMF = DSCD / VCD \quad (4)$$

The VCD represents the vertical column density, the vertically integrated concentration, which can be calculated from vertical profiles of temperature and pressure. Note that in contrast to other trace gases the SCD and VCD of O_4

Atmos. Meas. Tech. Discuss., doi:10.5194/amt-2016-148, 2016
Manuscript under review for journal Atmos. Meas. Tech.
Published: 30 May 2016

are expressed relative to the square of the O_2 concentration (see Greenblatt et al., 1990). For the measurements during the CINDI campaign the O_4 VCD is determined as $1.41 \cdot 10^{43}$ molecules²/cm⁵ (Wagner et al., 2014).

To obtain the total O_4 AMF of the measurement the O_4 AMF of the FRS (AMF_{FRS}) has to be added:

$$AMF = DAMF + AMF_{FRS} \tag{5}$$

The determination of AMF_{FRS} and application of equation 5 constitutes the calibration of the O_4 measurements. In the following we describe how AMF_{FRS} can be determined. Figure 5 presents simulated O_4 AMFs for (near) zenith view for different cloud-free (coloured lines) and cloudy conditions (black lines). From these simulation results two important findings can be deduced:

a) Around SZA of 36° (indicated by the blue arrows) the O_4 AMFs for the different aerosol scenarios are almost the same.

b) For cloudy scenarios the O_4 AMF can be either decreased or increased compared to cloud-free scenarios: For low and optically thick clouds the O_4 AMFs are enhanced, while for high and optically thin clouds the O_4 AMFs are decreased (Wagner et al., 2011).

The first finding indicates that clear sky observations (around SZA of 36°) can in principle be used for the calibration of the O_4 measurements, even if the exact AOD is not known. The second finding indicates that cloudy measurements (as identified by CI) should be removed before the calibration is performed. Figure 6 presents a comparison of the measured O_4 DAMFs and simulated O_4 AMFs. Note that the y-axes were shifted by 1.78, the value, which was finally derived for the O_4 AMF of the FRS (see below). In the top panel, all measurements, and in the bottom panel only measurements for clear sky conditions are shown (the cloud filtering was performed using the CI as described in Wagner et al., 2014). Interestingly, not only for the cloud-filtered measurements, but also for all measurements the minimum O_4 DAMFs are well represented by the simulations (for clear sky) indicating that during the CINDI campaign situations with only high thin cloud layers did not occur. This finding is confirmed by results from LIDAR measurements (see Wagner et al., 2014). Of course, the probability of high clouds (without low clouds present at he same time) can be different for other seasons and locations. Thus we recommend that always a cloud filter should be applied to the measured O_4 DAMF, before they are compared to the simulated O_4 AMFs.

Figure 7 presents the measured O_4 DAMFs after the simulated O_4 AMFs for AOD of 0.2 were subtracted. This normalisation procedure is applied to the remove the SZA dependence from the O_4 AMF. The choice of the simulations for AOD of 0.2 is somehow arbitrary, but the exact choice has only a very small effect on the normalisation results. For the calibration of the O_4 DAMF, measurements for SZA between 30° and 50° were chosen for two reasons:

a) For different aerosol layer heights, the SZA for which the O_4 AMF for different AOD become similar varies slightly between about 30° (for layer heights of 500m) and 50° (for layer heights of 2000 m), see Fig. A1 in the appendix. Since the aerosol layer height is usually unknown and can vary with time, we chose a SZA range, which covers typical aerosol layer heights.

b) After applying the cloud filter, the number of measurements decreased by about a factor of 3. The rather large SZA range ensures that still a useful number of measurements is available for the comparison with the simulation results.

Atmos. Meas. Tech. Discuss., doi:10.5194/amt-2016-148, 2016
Manuscript under review for journal Atmos. Meas. Tech.
Published: 30 May 2016

In Fig. 8 the frequency distribution of the normalised O_4 DAMF is shown for all observations (blue) or only clear sky observations (red). The maximum values and uncertainties are determined in the same way as for the CI (section 2). For both cases (all measurements or clear sky measurements) a value for the O_4 AMF of the FRS (AMF_{FRS}) of 1.78 is derived. The uncertainties are ±0.09 and ±0.08 for all and clear sky observations, respectively. Here it should be noted that the rather large uncertainties are caused by the poor statistics and can probably be reduced if measurements for longer periods with more clear days are analysed. A very similar value for AMF_{FRS} (1.75) was also found by Wagner et al. (2014).

In Fig. 8 also results for MAX-DOAS observations at Wuxi (China) are shown (Wang et al., 2015). Measurements over a period from 1 January 2012 to 31 December 2012 were used. Like for the Cabauw measurements a clear peak is found indicating that the method works in a similar way for completely different locations and measurement conditions. The derived value for the O_4 AMF of the FRS is almost the same as for the Cabauw measurements caused by the fact that both FRS were recorded under similar conditions.

4 Determination of threshold values for the newly calibrated MAX-DOAS data

In this section we determine a new set of threshold values for cloud and aerosol classification based on the newly calibrated CI and O_4 AMF and compare the new cloud classification results with our original study (Wagner et al., 2014). In contrast to the original version of the cloud classification algorithm, the new threshold values are determined for well-defined atmospheric scenarios. Thus the procedures for the determination of the threshold values can be applied to any measurements at different locations and seasons. The new threshold values also better represent the SZA dependencies. Note that compared to the original cloud classification algorithm the measured radiance is not considered anymore, because the calibration procedure for the radiance is time consuming and requires well defined and stable atmospheric conditions (Wagner et al., 2015). Such conditions might be rare especially for rather short measurement periods. Also, for many measurement locations, no simultaneous sun photometer measurements are available. Fortunately, omitting the measured radiance from the classification scheme does not cause a significant loss of information, because optically thick clouds can also be identified using the measured O_4 DAMFs.

4.1 New threshold values for the CI

In the original cloud classification scheme the measured CI was first normalised (divided) by a SZA-dependent clear sky reference value (simulated for an AOD of 0.3). The normalisation was applied to correct the strong SZA dependence of the CI (see Fig. 1). Then a constant threshold (independent from the SZA) was used to discriminate clear from cloudy observations. However, it turned out that the simple normalisation was not sufficient for large SZA (> 60°). Thus we decided to use a SZA dependent threshold in the new version of our cloud classification algorithm (but we not apply the normalisation of the measured CI values anymore). As threshold values we use simulation results for AODs of 0.75 for 440 nm (CI_{orig}) and 0.85 for 390 nm (CI_{new}), respectively. The AOD value for 440nm was chosen to achieve consistency between the new and the original classification scheme (for small SZA). The

Atmos. Meas. Tech. Discuss., doi:10.5194/amt-2016-148, 2016
Manuscript under review for journal Atmos. Meas. Tech.
Published: 30 May 2016

Atmospheric Measurement Techniques Discussions

corresponding AOD values at the other wavelengths (including those for the calculation of CI_{new}) were derived from the AOD at 440 nm using a typical Ångstrøm exponent of unity.

In Fig. 9 the calibrated CI_{orig} and CI_{new} for 24 June 2009 are compared to simulated CI for different aerosol and cloud properties. Note that the CI for AOD represents the SZA dependent threshold value, see Tables 1 and A1. During the morning the measured CI are similar to the simulation results for the AOD obtained from the simultaneous AERONET measurements. Around noon, the AOD increases and also some clouds appear. As a consequence the measured CI decreases and at several times it even falls slightly below the simulated minimum values. After about 15:00 the clouds disappear, but the CI stays at low levels because of the increased AOD in the afternoon.

In Fig. 10 the fractions of clear sky observations using the new thresholds for CI_{orig} and CI_{new} are compared to the results of the original algorithm. For all versions of the algorithms the fraction of clear sky observations increases with increasing SZA (but for CI_{new} a slight decrease is also found for SZA > 75°). In Fig. 10 also the fraction of clear sky conditions based on AERONET observations (level 2 data) is shown. Since AERONET observations require direct sunlight, fraction of clear sky conditions is simply determined as fraction of available measurements per SZA interval. Also the AERONET results indicate an increasing fraction of clear sky conditions with increasing SZA, which qualitatively confirms the MAX-DOAS results.

Finally, it should also be noted that a change of the calibration of the CI by ±2% (see section 2) leads to a change of the fraction of the clear sky measurements of ±4%.

Polynomial expressions describing the SZA dependent threshold values for zenith viewing direction are provided in Table 1; tabulated values are provided in Table A1 in the appendix.

4.2 New threshold values for the Temporal Smoothness Indicator TSI

In our original algorithm a so-called temporal smoothness indicator (TSI) is used, which is derived from the temporal variability of of the CI (for details see Wagner et al., 2014). It is used to identify rapid variations of the sky conditions, e.g. related to broken clouds. In our original study, the TSI was normalised (divided) by the clear sky reference value and a constant threshold was applied to discriminate measurements with high TSI from measurements with low TSI (indicating a smooth temporal variation of the CI). In the new version the TSI values are not nomalised by the clear sky values, but instead a SZA dependent threshold value is used. The advantage of this approach is that the threshold values can be calculated based on well-defined atmospheric scenarios. Here we suggest again to use a clear sky scenario with moderate aerosol load (AOD of 0.2) and the minimum CI for cloudy conditions (see Fig. 9). The AOD of 0.2 is assumed for the upper wavelength and the AOD for the lower wavelength is calculated assuming an Angstrom exponent of 1. The threshold value is calculated from the CI for both scenarios:

$$TSI_{threshold}(SZA) = \alpha * CI_{diff}(SZA) = \alpha * [CI_{AOD=0.2}(SZA) - CI_{min}(SZA)] \quad (6)$$

Here $TSI_{threshold}(SZA)$ represents the threshold value and $CI_{diff}(SZA)$ is the difference of the simulated CI for clear and cloudy conditions. We chose the proportionality constant α such that for SZA around 50° the threshold value for the new version of the algorithm matches that of the original version. The corresponding polynomial expression for

$TSI_{threshold}$(SZA) for exact zenith view is provided in Table 1, and tabulated values are provided in Table A1 in the appendix.

It should be noted that in contrast to the other parameters, for the TSI no universal threshold (that means no universal value for α) can be provided, because the TSI depends not only on the temporal variation of the colour of the sky, but also systematically on the integration time and the temporal distance between two successive measurements. Both parameters are different for individual instruments. It might be an interesting task for future studies to derive a parameterisation of α as a function of both parameters (and the cloud properties and wind fields).

In this study we do not provide a set of thresholds for the TSI in non-zenith viewing directions, because they also depend on the azimuth angle, which is different for different instruments (and seasons). Fig. 11 presents the SZA dependent fractions of observations with TSI above the threshold value for the different versions of or algorithm. Except for high SZA good agreement is found. Here it should also be noted that a change of the calibration of the CI by ±2% (see section 2) leads to a change of the fraction of measurements for which the TSI exceeds the threshold of ±0.5%.

4.3 New threshold values for the spread of the CI for different elevation angles

The spread of the CI for the different elevation angles approaches zero in the presence of clouds (Wagner et al., 2014), which makes it a useful quantity for the distinction between situations with enhanced aerosol loads or clouds. This is an important option for cases which can not be distinguished based on the absolute value of the CI. We quantify the spread of the CI by calculating the difference between the maximum and minimum CI for all elevation angles of individual elevation sequences. The results of simulated values of the spread of CI_{orig} and CI_{new} for different aerosol and cloud scenarios as well as for different SZA and relative azimuth angles (see Figs. A2 and A3 in the appendix) indicate that the spread of the CI depends systematically on the SZA but also on the relative azimuth angle. Thus a simple normalisation as function of the SZA is in general not appropriate (while for selected measurements with a specific relation between the SZA and the relative azimuth angle it might still be useful). Our simulations also indicate that clouds and aerosols (with the same optical depth) have a very similar effect on the spread of the CI (the differences are mainly a result of the different wavelength dependence of cloud and aerosol scattering). Thus in many cases, it will be difficult to clearly discriminate between both types of atmospheric scatterers based on the spread of the CI. Nevertheless, cases with high optical depth (about > 6) can be still clearly identified based on the used threshold of 0.14.

It is recommended that future studies should investigate which SZA dependent threshold values could be used for specific measurements (with fixed relationships between SZA and relative azimuth angle). In this way the discrimination between measurements with high and low optical depth might be improved compared to the use of a fixed threshold. Also the CI from the individual elevation angles should be used in a more sophisticated way, e.g. by using individual threshold values for all elevation angles.

Because of the complex dependence of the spread of the CI on the viewing geometry, in this study we used a constant threshold of 0.14. In Fig. 12 the fraction of measurements with spread of the CI above the threshold are shown for CI_{orig} and CI_{new} using the different versions of the algorithm. Except for high SZA good agreement is found

A change of the calibration of the CI by ±2% (see section 2) leads to a change of the fraction of measurements with spread of the CI above the threshold of ±0.5%.

4.3.1 Possibilities to distinguish between the effects of clouds and aerosols with different optical depths

As discussed in the previous section, from measurements of the absolute value of the CI alone it is difficult to distinguish between aerosols and clouds if they have the same optical thickness (especially for optical thicknesses between about 1 and 6). This is especially important for the presence of continuous clouds, because they cannot be detected by enhanced values of the temporal smoothness indicator. Here observations of the O_4 absorption are useful, because they are sensitive to the layer height of atmospheric scatterers, which is usually different for aerosols and clouds. The simplest possibility would be to identify clouds by increased differences between the measured O_4 absorptions and the corresponding results of the forward model (if clouds are not explicitly included in the forward model). Alternatively, a simple parameterisation of clouds might also be included in the forward model. Then clouds could be identified by a retrieved elevated layer. Here it should be noted that clouds might also be located close to the surface (fog), and also aerosols might be located at elevated altitudes. In such cases, the retrieval algorithm can probably not distinguish between both types of scatterers. As a consequence the derived extinction profiles might be systematically wrong if aerosol optical properties are used for a cloud scenario or vice versa. However, for the trace gas retrieval this is usually not a problem, as long as a consistent aerosol/cloud model is used for the aerosol profile retrieval and the trace gas profile retrieval.

4.4 Threshold for the O_4 AMF in zenith direction

Like in the original version of the algorithm, the SZA dependence of the measured O_4 AMFs is corrected by subtracting the corresponding clear sky reference values. But the clear sky reference value is now calculated for an AOD of 0.2 to be in agreement with the AERONET observations on 24 June 2009. The corrected O_4 AMFs are then compared to a constant threshold value. Because of the new calibration (section 3) and the new clear sky reference values, a slightly different threshold value (0.85) compared to the original algorithm (0.80) is applied. Fig. 13 compares the results of the different versions of the algorithm, and very similar results are found.
It should also be noted that a change of the calibration of the O_4 AMF by ±0.08 (see section 3) leads to a change of the fraction of measurements classified as under thick clouds ±1.5%.

4.4.1 Estimation of a SZA dependent threshold for the radiance

As mentioned before, the calibration of the radiance requires more effort than the calibration of the CI and O_4 absorption. In particular, measurements for days with constant and well known AOD are required (Wagner et al., 2015). Thus the updated version of the cloud classification scheme does not use the measured radiance for the detection of optically thick clouds, because such clouds can also be well identified by the O_4 absorption observed in zenith direction. Nevertheless, in some cases, especially for long term observations, the use of O_4 observations for the detection of optically thick clouds might be strongly affected by instrumental degradation (Wang et al., 2015). For such cases it might still be useful to identify optically thick clouds based on the measured radiance. Thus, in this subsection we propose a simple method for the determination of a threshold value, which can be applied to the uncalibrated radiance. It is based on the comparison of measured radiances for optically thick and thin clouds as determined from the O_4 absorption. In Fig. 14 all radiance observations for optically thin clouds (identified by the O_4 absorption) are indicated by red dots, and measurements for optically thick clouds by blue dots. In spite of some 'outliers', the transition between thin and thick clouds (as a function of the SZA) can be clearly identified. Moreover, the threshold value used in the original version of the algorithm (indicated by the black line) fits well to the transition between the red and blue points. This finding indicates the possibility to determine the threshold value for the radiance without performing an explicit radiance calibration of the instrument via the relationship with the observed O_4 absorption in zenith direction. In section 4.7 a strategy is outlined how the combination of O_4 and radiance measurements could be combined for long term measurements.

4.5 Threshold for the spread of the O_4 AMF

The calculation of the spread of the O_4 AMF for the different elevation angles is not affected by the new calibration, since the same offset value is added to the O_4 DAMF of all elevation angles. Thus the same threshold value as in the original version (0.37) is still used and there are no changes of the results for the identification of fog.

4.6 Threshold values for observations at exactly zenith direction (elevation angle of 90°)

Since for our MAX-DOAS measurements during the CINDI campaign the 'zenith observations' were not performed in exactly zenith direction (but instead at an elevation angle of 85°), the question arises whether the threshold values can be also used for observations in exact zenith direction. In Figs. 15 and 16 the threshold values for the CI and the O_4 absorption (based on the defined atmospheric scenarios) are compared for and elevation angle of 85° and exact zenith view. For the CI the differences of the CI are typically < 10% (the minimum values are almost identical). Thus we conclude that the findings for our measurements can be directly transferred to observations in exact zenith direction. The same conclusions hold for the quantities derived from the CI, the TSI and the spread of the CI (see also Figs. A2 and A3 in the appendix). In Fig. 16 the clear sky reference values of the O_4 AMF for elevation angles of 85° and 90° are compared. Almost identical values are found indicating that the reference value for 85° can also be used for measurements at exactly zenith view. Polynomial expressions for all threshold values for exact zenith direction are provided in Table 1; tabulated values are provided in Table A1 in the appendix.

4.7 Effect of instrumental degradation for long term measurements

Especially for long term measurements instrumental degradation can become an important issue, because the results of the CI, O_4 absorption (and radiance) might systematically change over time. Wang et al. (2015) presented a method to quantify and correct the effect of instrument degradation using time series of the derived quantities for the same viewing geometry. They also suggested a degradation correction for the observed CI and radiance. Unfortunately, for O_4 absorption the effect of instrumental changes (in particular the change of the instrument's resolution) can be very strong, and usually these influences cannot be corrected well. Thus the use of the O_4 absorption for the detection of optically thick clouds can become a particular problem for long term measurements.

Thus for long term observations the occurrence of optically thick clouds should probably be based on observations of the radiance. An approach for an 'indirect' calibration of the radiance was suggested in section 4.4.1. This method could be applied for periods, in which the effect of instrumental changes on the O_4 absorption are negligible. The derived radiance calibration could then be used for the entire period of the MAX-DOAS measurements.

5 Peculiarities for measurements at high and low latitudes

5.1 Observations at low latitudes

The results in Fig. 15 indicate a potential problem for measurements at low SZA (< about 30°). For such viewing geometries the difference of the CI for clear and cloudy observations decreases, and the CI for cloudy situations can even become larger than the threshold values for the detection of high aerosol loads or clouds. Thus the identification of cloudy measurements for low SZA becomes increasingly uncertain or eventually even impossible based on the absolute value of the CI. For such situations, it is recommended to identify clouds by the spread of the CI as proposed by Wang et al. (2015).

5.2 Observations at high latitudes

The application of the cloud classification scheme at high latitudes is subject to two specific problems. First, measurements at small SZA are rare. This problem mainly affects the calibration of the O_4 absorption. Second, the surface will be covered by snow and ice during large parts of the year. Increased values of the surface albedo strongly affect the atmospheric radiative transport and thus probably also the proposed calibration approaches and derived threshold values.

Figure 17 shows simulated CI and O_4 AMFs in zenith direction for high surface albedo (0.8). Interestingly, the CI is hardly affected by the increase of the surface albedo: Compared to the results for low surface albedo (Fig. 15, bottom), the CI values are shifted towards slightly higher values by an almost constant value, indicating the effect of increased multiple scattering, which also leads to more Rayleigh scattering events of the observed photons. These results indicate that for measurements over snow and ice-covered surfaces a similar calibration approach for the CI as for measurements over low albedo can be applied.

In contrast, the O_4 AMFs (Fig. 17 bottom) are strongly affected by the increased surface albedo. Compared to the results for low surface albedo (Fig. 5), systematically higher values are found. Moreover, for SZA < 80° the O_4 AMF depend strongly on the AOD. From these findings we conclude that the calibration method developed for measurements above small surface albedo has to be modified before it can be applied to measurements over high surface albedo. Probably clear sky measurements at large SZA (around 80°) can be used for the comparison of measured and simulated O_4 AMF. Fortunately, this possibility fits well to the fact that at high latitudes most measurements are performed at moderate to high SZA.

These simulation results indicate that for measurements at high latitudes modified calibration approaches and threshold values would have to be used. The details of these modifications need to be tested in more detail. Here it should also be considered that especially in spring and autumn the surface albedo often changes rapidly. Thus also

Atmos. Meas. Tech. Discuss., doi:10.5194/amt-2016-148, 2016
Manuscript under review for journal Atmos. Meas. Tech.
Published: 30 May 2016

methods for the detection (and quantification) of changes of the surface albedo based on the MAX-DOAS observations should be developed.

6 Conclusions and outlook

We developed methods for the calibration of the colour index (CI) and the O_4 absorption derived from (MAX-) DOAS measurements of scattered sunlight, which are an important step towards a universal cloud classification scheme for MAX-DOAS observations. Both calibration methods are based on the comparison of measurements and radiative transport simulations for well-defined atmospheric conditions (e.g. clear or cloudy conditions) and limited SZA ranges.

For the calibration of the CI observations under cloudy conditions are used, for which minimum values of the CI are found (if the CI is defined as the ratio of the intensity at the short wavelength divided by the intensity at the long wavelength). The result of the calibration procedure is a proportionality constant, which is applied to the measured CI.

For the calibration of the O_4 absorption observations under clear sky conditions and for a limited SZA range are used. As a result of the calibration procedure a constant offset is determined (the O_4 absorption of the Fraunhofer reference spectrum), which is added to the measured O_4 absorption. We successfully applied both calibration methods to measurements at two locations: Cabauw in the Netherlands, and Wuxi in China.

In the second part of our study we applied the cloud classification algorithm described in Wagner et al. (2014) to the calibrated CI and O_4 absorptions and adapted the original threshold values accordingly. Together with the calibration method, the new set of threshold values can be used in a consistent way for any MAX-DOAS measurement thus constituting a universal method for cloud classification. In addition to the new threshold values the updated version of the cloud classification includes further important improvements:

a) we used a new wavelength pair (330 nm / 390 nm) for the CI. Compared to the CI (320 nm / 440 nm) used in our original study (Wagner et al., 2014) this choice has two advantages: The change of the low wavelength to 330 nm largely minimises the impact of the ozone absorption on the CI. The change of the upper wavelength to 390 nm ensures that the new CI can be calculated for almost all UV (MAX-) DOAS instruments (which often do not cover 440 nm).

b) The new threshold values better describe the SZA dependence. They are obtained from radiative transfer simulations for well-defined atmospheric scenarios. This aspect is important, since it ensures that threshold values for possible modified CI or additional cloud-sensitive quantities could be determined in a consistent way (based on the same atmospheric scenarios).

c) No radiance measurements are used in the new version, because the absolute calibration of the measured radiance spectra is more complicated than those of the CI and the O_4 absorption. Fortunately, the omission of the radiance measurements has no large impact on the classification results, because the radiance was only used for the detection of optically thick clouds, which can also well be identified from the O_4 absorption.

We compared the results of the updated cloud classification scheme with those from the original version and found in general good agreement.

It should be noted that our cloud classification algorithm is optimised for MAX-DOAS measurements at mid latitudes. For measurements at high and low latitudes specific problems occur: at low latitudes, many measurements are performed for small SZA, for which the CI becomes indistinguishable for clear and cloudy conditions. As suggested by Wang et al. (2015) this problem can be partly overcome by the use of the spread of the CI for the identification of clouds. At high latitudes, measurements at small SZA are rare, which can lead to problems for the application of the calibration methods, especially for the O_4 absorption. In addition, frequently increased surface albedo due to snow and ice strongly affect the atmospheric radiative transfer and thus the prerequisites of our calibration methods. However, sensitivity studies suggest that for such conditions modified versions of the calibration methods and cloud classification scheme can still be applied.

Another problem of the new version of the algorithm is that especially for long term observations the derived O_4 absorptions might be strongly affected by temporal changes of the instrument properties. Thus the identification of optically thick clouds might be impossible for such measurements. As a possible solution for this limitation we propose a new indirect determination of the threshold value for the uncalibrated radiance, which is based on the O_4 measurements for periods which are not affected by instrumental changes. Optically thick clouds could then be identified based on the uncalibrated radiances, which are usually less affected by instrument degradation (and can be better corrected for instrumental changes than the O_4 absorption).

Finally we identify important research areas, which should be addressed in future studies in order to further improve the cloud classification scheme. These areas include the determination of correction factors for the temporal smoothness indicator (depending on the integration time and time difference of successive measurements), a more sophisticated use of CI derived from individual elevation angles, modifications for the cloud classification algorithm for situations with high surface albedo as well as the investigation of 3D cloud effects on the CI.

Acknowledgments

We want to thank the organisers of the Cabauw Intercomparison Campaign of Nitrogen Dioxide measuring Instruments (CINDI) campaign in Summer 2009 (http://www.knmi.nl/samenw/cindi/), especially Ankie Piters and Marc Kroon. We thank J.S. (Bas) Henzing and his staff for his effort in establishing and maintaining the Cabauw AERONET site used in this investigation.

Tables

Table 1 Polynomial expressions for the SZA dependent thresholds of the different quantities.

Quantity	Polynomial as function of the SZA (S)
CI (320 nm / 440 nm)	$y = 0.000000001467636*S^5 - 0.00000024941575*S^4 + 0.0000090594954*S^3 + 0.000057323819*S^2 + 0.0020017837*S + 0.54041811$
CI (330 nm / 390 nm)	$y = -0.0000000027478517*S^5 + 0.000000074955919*S^4 - 0.0000098789109*S^3 + 0.00047634128*S^2 - 0.0013021066*S + 0.77903017$
TSI CI (320 nm / 440 nm)	$y = 5.3005E-16*S^5 - 8.973983E-14*S^4 + 0.000000000003629323*S^3 + 0.00000000000003443889*S^2 + 0.0000000001852435*S + 0.00000007311181$
TSI CI (330 nm / 390 nm)	$y = 5.3868552E-18*S^6 - 1.1463286E-15*S^5 + 9.1108209E-14*S^4 - 0.0000000000041592073*S^3 + 0.00000000012014659*S^2 - 0.0000000066964031*S + 0.000000063744804$
Spread CI (320 nm / 440 nm)	constant value: 0.14
Spread CI (330 nm / 390 nm)	constant value: 0.14
O_4 AMF zenith	$y = -1.54250282E-10*S^6 + 3.34931093E-08*S^5 - 2.63143730E-06*S^4 + 8.84531202E-05*S^3 - 9.66971367E-04*S^2 + 1.07098542E-02*S + 1.26521523E+00$
Spread of the O_4 DAMF	constant value: 0.37

References

Clémer, K., Van Roozendael, M., Fayt, C., Hendrick, F., Hermans, C., Pinardi, G., Spurr, R., Wang, P., and De Mazière, M.: Multiple wavelength retrieval of tropospheric aerosol optical properties from MAXDOAS measurements in Beijing, Atmos. Meas. Tech., 3, 863-878, doi:10.5194/amt-3-863-2010, 2010.

Frieß, F., P. S. Monks, J. J. Remedios, A. Rozanov, R. Sinreich, T. Wagner, and U. Platt, MAX-DOAS O4 measurements: A new technique to derive information on atmospheric aerosols. (II) Modelling studies, J. Geophys. Res., 111, D14203, doi:10.1029/2005JD006618, 2006.

Gielen, C., Van Roozendael, M., Hendrick, F., Pinardi, G., Vlemmix, T., De Bock, V., De Backer, H., Fayt, C., Hermans, C., Gillotay, D., and Wang, P.: A simple and versatile cloud-screening method for MAX-DOAS retrievals, Atmos. Meas. Tech., 7, 3509-3527, doi:10.5194/amt-7-3509-2014, 2014.

Grainger, J.F., and J. Ring, Anomalous Fraunhofer line profiles, Nature, 193, 762, 1962.

Greenblatt G.D., Orlando, J.J., Burkholder, J.B., and Ravishankara, A.R.: Absorption measurements of oxygen between 330 and 1140 nm, J. Geophys. Res., 95, 18577-18582, 1990.

Heckel, A., A. Richter, T. Tarsu, F. Wittrock, C. Hak, I. Pundt, W. Junkermann, and J. P. Burrows, MAX-DOAS measurements of formaldehyde in the Po-Valley, Atmos. Chem. Phys., 5, 909-918, 2005.

Hendrick, F., Müller, J.-F., Clémer, K., Wang, P., De Mazière, M., Fayt, C., Gielen, C., Hermans, C., Ma, J. Z., Pinardi, G., Stavrakou, T., Vlemmix, T., and Van Roozendael, M.: Four years of ground-based MAX-DOAS observations of HONO and NO_2 in the Beijing area, Atmos. Chem. Phys., 14, 765-781, doi:10.5194/acp-14-765-2014, 2014.

Hönninger G., and Platt U., Observations of BrO and its vertical distribution during surface ozone depletion at Alert, Atmos. Environ., 36, 2481–2490, 2002.

Hönninger, G., von Friedeburg, C., and Platt, U.: Multi Axis Differential Optical Absorption Spectroscopy (MAX-DOAS), Atmos. Chem. Phys., 4, 231–254, 2004, http://www.atmos-chem-phys.net/4/231/2004/.

Irie, H., Kanaya, Y., Akimoto, H., Iwabuchi, H., Shimizu, A., and Aoki, K.: First retrieval of tropospheric aerosol profiles using MAX-DOAS and comparison with lidar and sky radiometer measurements, Atmos. Chem. Phys., 8, 341-350, doi:10.5194/acp-8-341-2008, 2008.

Li, X., Brauers, T., Shao, M., Garland, R. M., Wagner, T., Deutschmann, T., and Wahner, A.: MAX-DOAS measurements in southern China: retrieval of aerosol extinctions and validation using ground-based in-situ data, Atmos. Chem. Phys., 10, 2079-2089, doi:10.5194/acp-10-2079-2010, 2010.

Ma, J. Z., Beirle, S., Jin, J. L., Shaiganfar, R., Yan, P., and Wagner, T.: Tropospheric NO_2 vertical column densities over Beijing: results of the first three years of ground-based MAX-DOAS measurements (2008–2011) and satellite validation, Atmos. Chem. Phys., 13, 1547-1567, doi:10.5194/acp-13-1547-2013, 2013.

Piters, A. J. M., Boersma, K. F., Kroon, M., Hains, J. C., Van Roozendael, M., Wittrock, F., Abuhassan, N., Adams, C., Akrami, M., Allaart, M. A. F., Apituley, A., Beirle, S., Bergwerff, J. B., Berkhout, A. J. C., Brunner, D., Cede, A., Chong, J., Clémer, K., Fayt, C., Frieß, U., Gast, L. F. L., Gil-Ojeda, M., Goutail, F., Graves, R., Griesfeller, A., Großmann, K., Hemerijckx, G., Hendrick, F., Henzing, B., Herman, J., Hermans, C., Hoexum, M., van der Hoff, G. R., Irie, H., Johnston, P. V., Kanaya, Y., Kim, Y. J., Klein Baltink, H., Kreher, K., de Leeuw, G., Leigh, R., Merlaud, A., Moerman, M. M., Monks, P. S., Mount, G. H., Navarro-Comas, M., Oetjen, H., Pazmino, A., Perez-Camacho, M., Peters, E., du Piesanie, A., Pinardi, G., Puentedura, O., Richter, A., Roscoe, H. K., Schönhardt, A., Schwarzenbach, B., Shaiganfar, R., Sluis, W., Spinei, E., Stolk, A. P., Strong, K., Swart, D. P. J., Takashima, H., Vlemmix, T., Vrekoussis, M., Wagner, T., Whyte, C., Wilson, K. M., Yela, M., Yilmaz, S., Zieger, P., and Zhou, Y.: The Cabauw Intercomparison campaign for Nitrogen Dioxide measuring Instruments (CINDI): design, execution, and early results, Atmos. Meas. Tech., 5, 457-485, doi:10.5194/amt-5-457-2012, 2012.

Sarkissian, A., Pommereau, J.-P., and Goutail, F., Identification of polar stratospheric clouds from the ground by visible spectrometry, Geophys. Res. Lett., 18, 779–782, 1991.

Sarkissian, A., Pommereau, J., Goutail, F., and Kyrö, E., PSC and volcanic aerosol observations during EASOE by UV-visible ground-based spectrometry, Geophys. Res. Lett., 21, 1319–1322, 1994.

Vlemmix, T., Hendrick, F., Pinardi, G., De Smedt, I., Fayt, C., Hermans, C., Piters, A., Wang, P., Levelt, P., and Van Roozendael, M.: MAX-DOAS observations of aerosols, formaldehyde and nitrogen dioxide in the Beijing area: comparison of two profile retrieval approaches, Atmos. Meas. Tech., 8, 941-963, doi:10.5194/amt-8-941-2015, 2015.

Wagner, T., B. Dix, C.v. Friedeburg, U. Frieß, S. Sanghavi, R. Sinreich, and U. Platt, MAX-DOAS O_4 measurements – a new technique to derive information on atmospheric aerosols. (I) Principles and information content, J. Geophys. Res., 109, D22205, doi: 10.1029/2004JD004904, 2004.

Wagner, T., Beirle, S., Brauers, T., Deutschmann, T., Frieß, U., Hak, C., Halla, J. D., Heue, K. P., Junkermann, W., Li, X., Platt, U., and Pundt-Gruber, I.: Inversion of tropospheric profiles of aerosol extinction and HCHO and NO2 mixing ratios from MAX-DOAS observations in Milano during the summer of 2003 and comparison with independent data sets, Atmos. Meas. Tech., 4, 2685-2715, doi:10.5194/amt-4-2685-2011, 2011.

Wagner, T., Apituley, A., Beirle, S., Dörner, S., Friess, U., Remmers, J., and Shaiganfar, R.: Cloud detection and classification based on MAX-DOAS observations, Atmos. Meas. Tech., 7, 1289-1320, doi:10.5194/amt-7-1289-2014, 2014.

Wagner, T., Beirle, S., Dörner, S., Penning de Vries, M., Remmers, J., Rozanov, A., and Shaiganfar, R.: A new method for the absolute radiance calibration for UV–vis measurements of scattered sunlight, Atmos. Meas. Tech., 8, 4265-4280, doi:10.5194/amt-8-4265-2015, 2015.

Wang, T., Hendrick, F., Wang, P., Tang, G., Clémer, K., Yu, H., Fayt, C., Hermans, C., Gielen, C., Müller, J.-F., Pinardi, G., Theys, N., Brenot, H., and Van Roozendael, M.: Evaluation of tropospheric SO_2 retrieved from MAX-DOAS measurements in Xianghe, China, Atmos. Chem. Phys., 14, 11149-11164, doi:10.5194/acp-14-11149-2014, 2014.

Wang, Y., Penning de Vries, M., Xie, P. H., Beirle, S., Dörner, S., Remmers, J., Li, A., and Wagner, T.: Cloud and aerosol classification for 2.5 years of MAX-DOAS observations in Wuxi (China) and comparison to independent data sets, Atmos. Meas. Tech., 8, 5133-5156, doi:10.5194/amt-8-5133-2015, 2015.

Wittrock, F., H. Oetjen, A. Richter, S. Fietkau, T. Medeke, A. Rozanov, and J. P. Burrows, MAX-DOAS measurements of atmospheric trace gases in Ny-Ålesund, Atmos. Chem. Phys., 4, 955–966, 2004.

Atmos. Meas. Tech. Discuss., doi:10.5194/amt-2016-148, 2016
Manuscript under review for journal Atmos. Meas. Tech.
Published: 30 May 2016

Atmospheric Measurement Techniques
Discussions

Figures

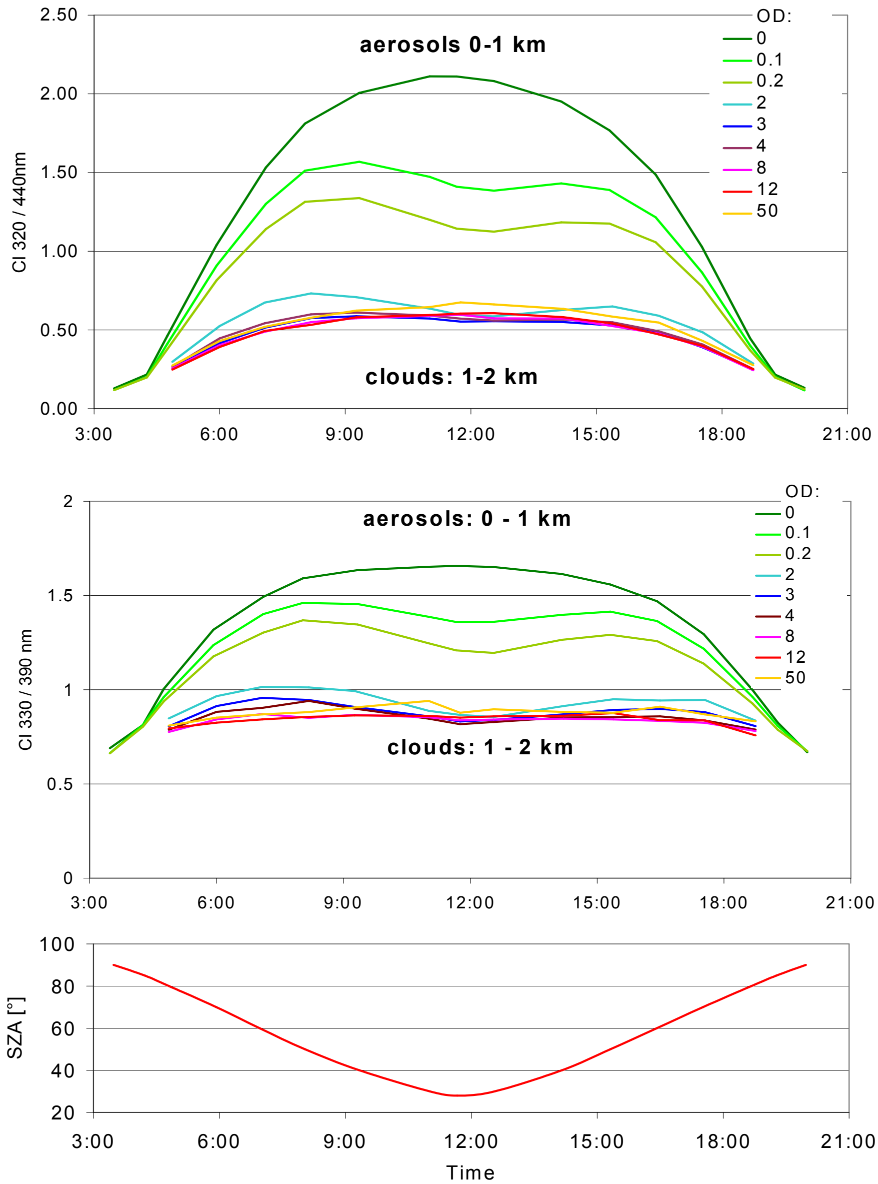

Figure 1: Simulated Colour indices for an elevation angle of 85° (top: $CI_{original}$ = 320 nm / 420 nm; middle: CI_{new} = 330 nm / 390 nm) for different aerosol and cloud optical depths. For the aerosol cases (green lines) the OD represents the value at 390 nm (Angstrom exponent = 1); for the cloud cases (OD≥2) the same optical depth is assumed for both wavelengths (Angstrom exponent = 0). The aerosol layer is between the surface and 1 km; the cloud layer is between 1 and 2 km. Aerosol properties are described by a Heyey-Greenstein model with an Asymmetry parameter of 0.68 and a single scattering albedo of 0.95. Bottom: SZA for a day (26 June 2009) in the middle of the campaign.

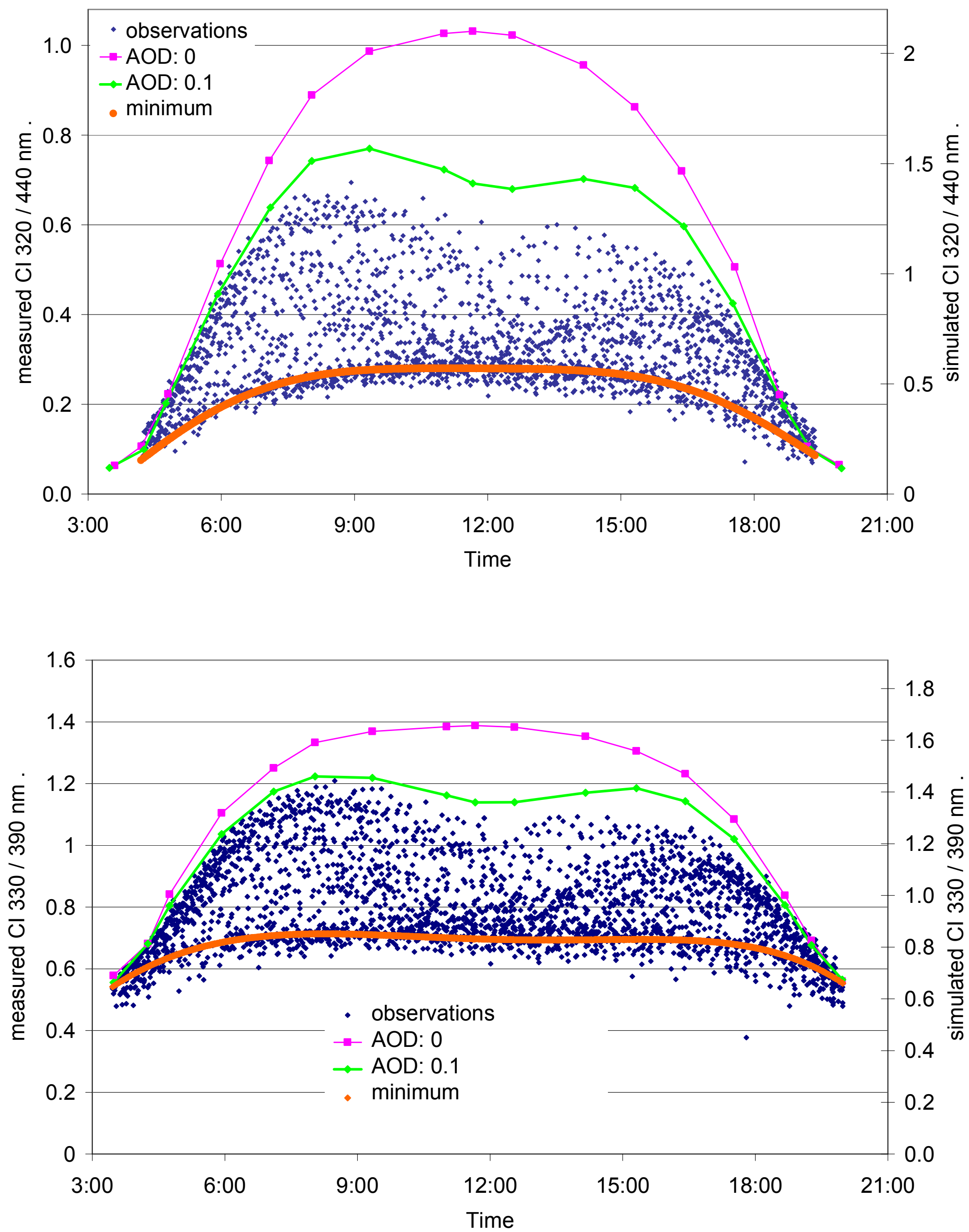

5 **Figure 2: Comparison of measured (left axis) and simulated CI (top: 320 nm / 440 nm; bottom: 330 nm / 390 nm) during CINDI. The lines represent minimum values (see Fig. 1), aerosol-free conditions, and low aerosol load (AOD = 0.1). The measurements are from the period 12 June to 15 July 2009; the simulations are performed for a day (26 June 2009) in the middle of the campaign.**

Atmos. Meas. Tech. Discuss., doi:10.5194/amt-2016-148, 2016
Manuscript under review for journal Atmos. Meas. Tech.
Published: 30 May 2016

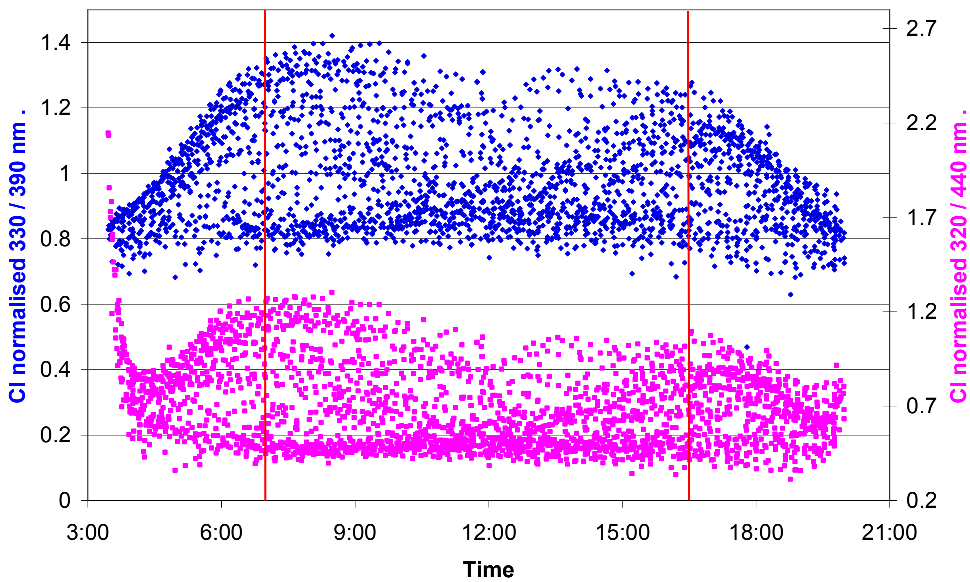

Figue 3: Normalised CI during CINDI for both wavelength pairs. The normalisation is performed by dividing the measured CI by the respective simulated minimum values. For SZA < 60° (indicated by the red vertical lines) the minima of the normalised CI are almost independent from the SZA. The measurements are from the period 12 June to 15 July 2009.

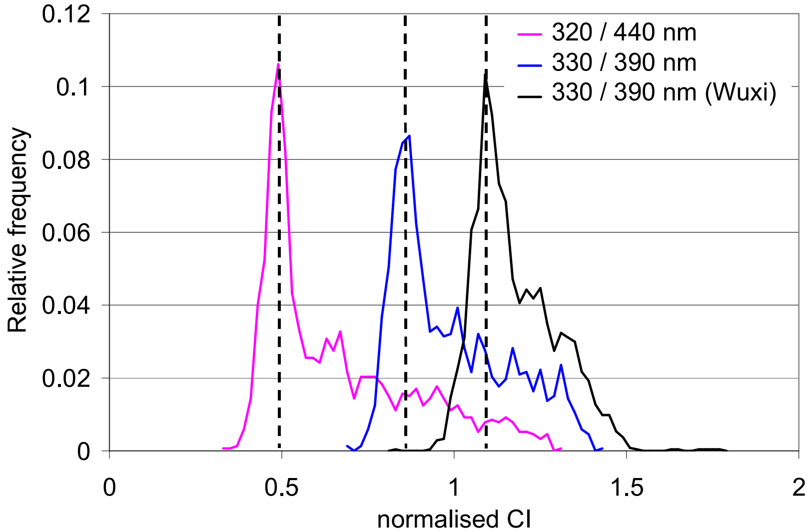

Figure 4: Frequency distribution of the normalised CI for SZA < 60° (for bins of 0.02). The blue and magenta curves represent the results for Cabauw (1527 measurements); the black curve represents the results for Wuxi (2440 measurements).

Atmos. Meas. Tech. Discuss., doi:10.5194/amt-2016-148, 2016
Manuscript under review for journal Atmos. Meas. Tech.
Published: 30 May 2016

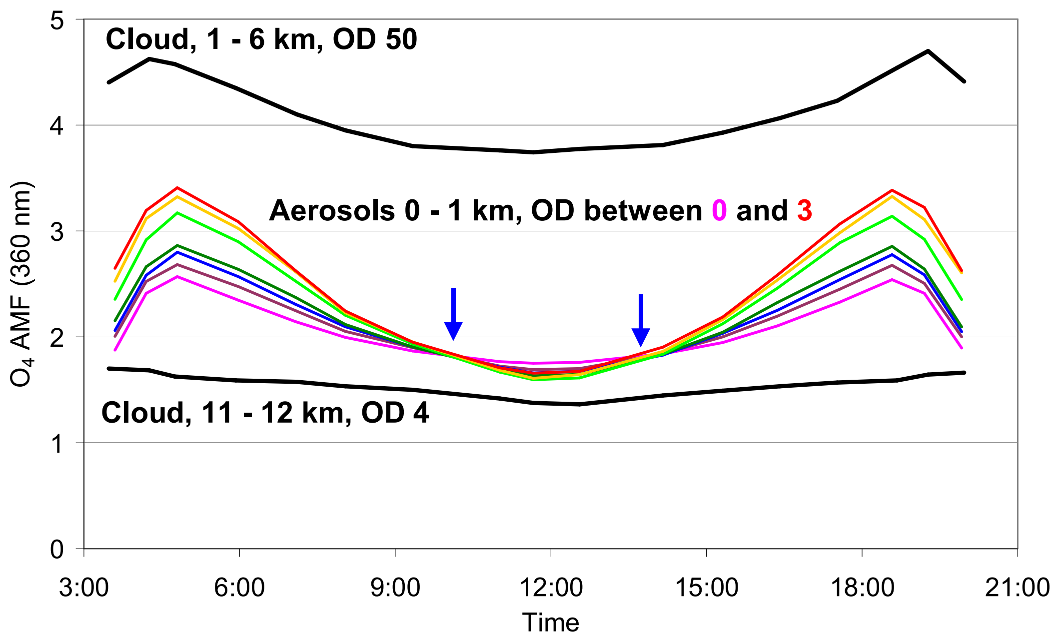

Figure 5: Simulated O_4 AMFs (360 nm) for different aerosol and cloud scenarios. The violet and red lines indicate results for minimum and maximum AOD of 0 and 3, respectively. For clear sky conditions almost the same O_4 AMFs are obtained around SZA of 36° (indicated by the blue arrows), independent from the assumed AOD. Depending on the cloud OD and the cloud height, clouds can either increase or decrease the O_4 AMF compared to clear sky conditions (Wagner et al., 2011). The simulations are performed for a day (26 June 2009) in the middle of the campaign.

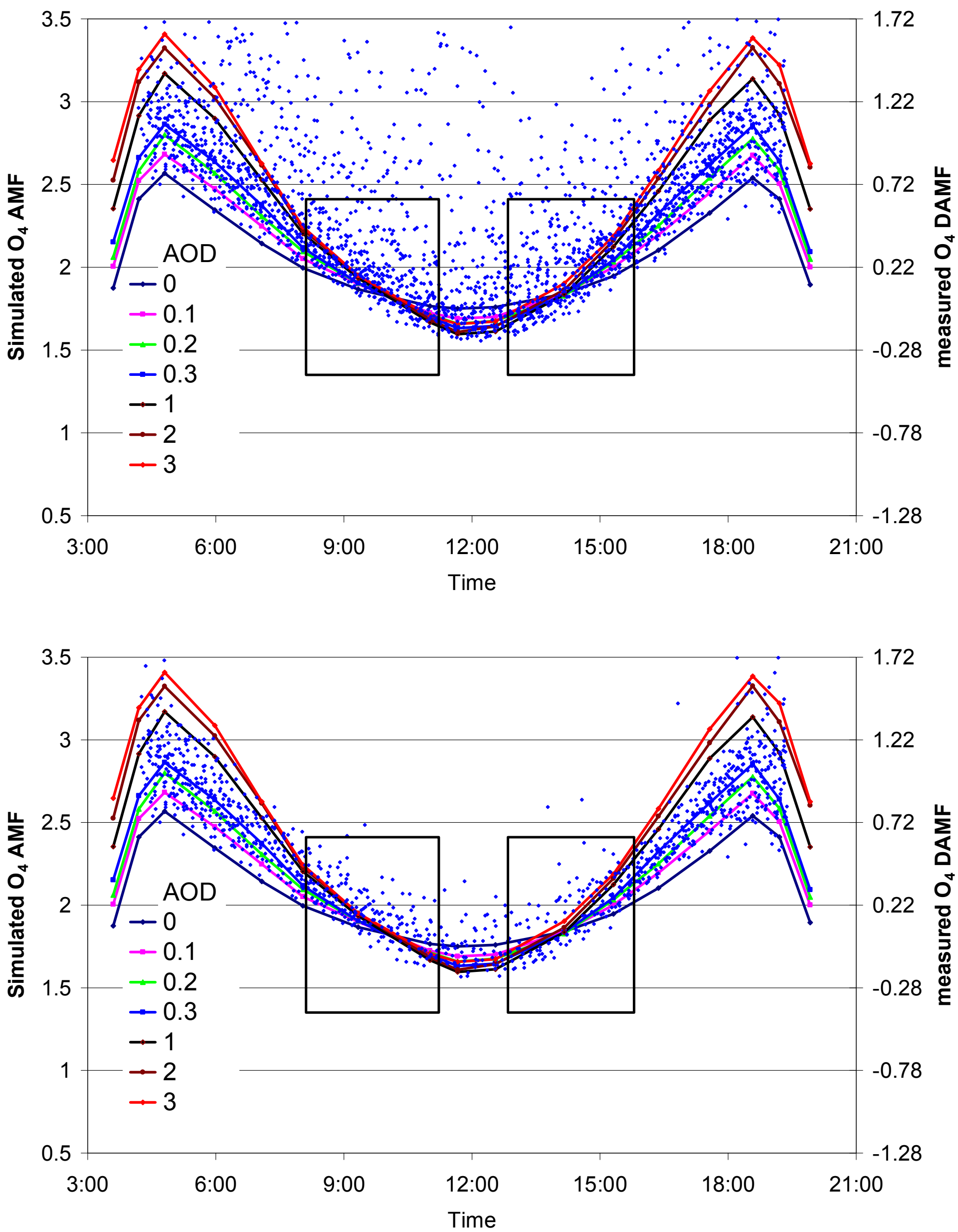

Figure 6: Comparison of measured O_4 DAMFs (right axis) with simulated O_4 AMFs (left axis) for different AOD. In the top panel all observations, and in the bottom panel only clear sky observations are shown. The rectangles indicate the SZA ranges (30° to 50°) used for the calibration of the O_4 measurements. The right y-axis is shifted compared to th eleft y-axis by the O_4 AMF of the FRS (-1.78). The measurements are from the period 12 June to 15 July 2009; the simulations are performed for a day (26 June 2009) in the middle of the campaign.

Atmos. Meas. Tech. Discuss., doi:10.5194/amt-2016-148, 2016
Manuscript under review for journal Atmos. Meas. Tech.
Published: 30 May 2016

Atmospheric Measurement Techniques Discussions

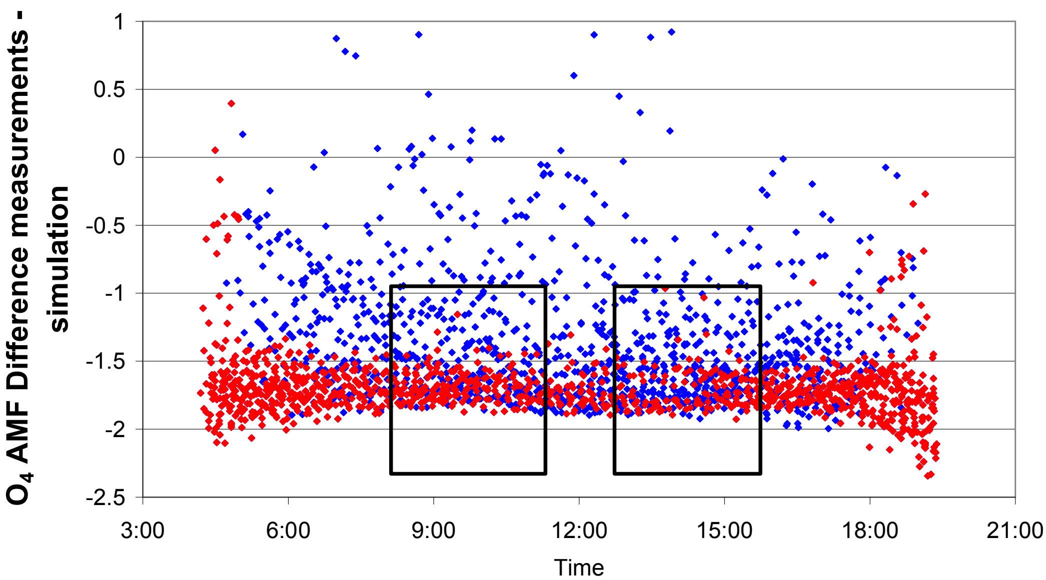

Figure 7: Normalised O_4 DAMF for all measurements (blue) or measurements under clear sky conditions (red). The normalisation is performed by subtracting the simulated O_4 AMFs for AOD of 0.2. The rectangles indicate the SZA ranges used for the calibration of the O_4 DAMF. The measurements are from the period 12 June to 15 July 2009.

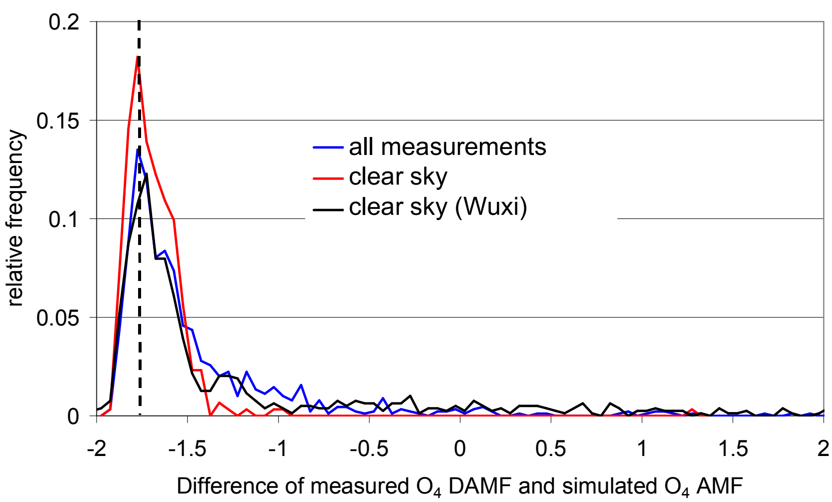

Figure 8: Frequency distribution (for bins of 0.05) of the normalised O_4 DAMF for SZA between 30° and 50°. The blue and red curves represents observations at Cabuw for all sky conditions (896 measurements) and clear sky conditions (302 measurements), respectively. For both selections the frequency maximum is found for –1.78. The black curve represents the frequency distribution for clear sky observations at Wuxi (790 measurements).

Atmos. Meas. Tech. Discuss., doi:10.5194/amt-2016-148, 2016
Manuscript under review for journal Atmos. Meas. Tech.
Published: 30 May 2016

Atmospheric Measurement Techniques
Open Access
Discussions

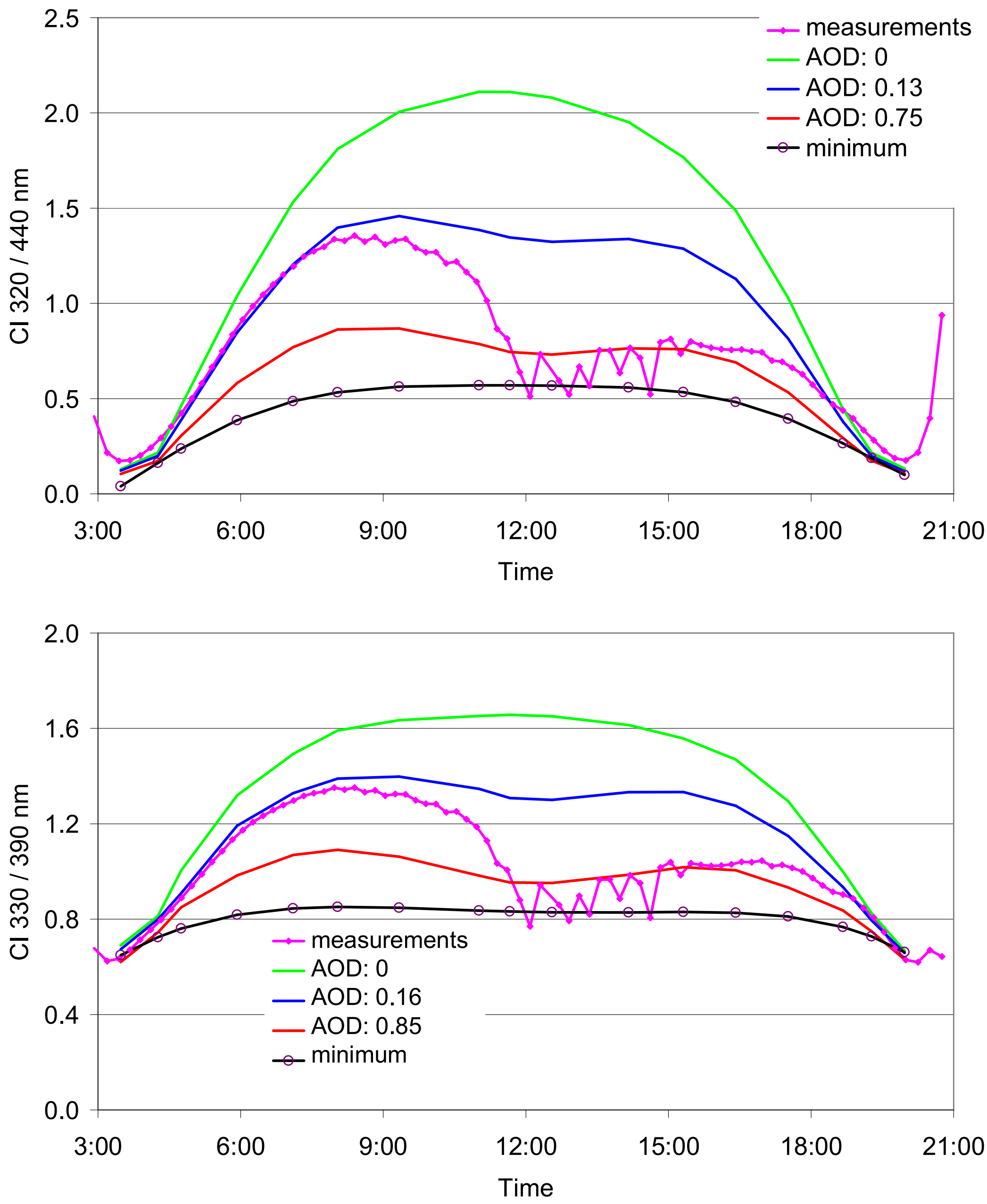

Figure 9: Comparison of measured CI for 24 June 2009 with simulated CI for different scenarios. Top: Original CI for 320 nm and 440 nm; Bottom: new CI for 330 nm / 390 nm. The AOD values in the legends correspond to the wavelengths 440 nm and 390 nm, respectively. The minimum values represent cloudy conditions (see Fig. 1). The the simulations are made for a day (26 June 2009) in the middle of the campaign.

Atmos. Meas. Tech. Discuss., doi:10.5194/amt-2016-148, 2016
Manuscript under review for journal Atmos. Meas. Tech.
Published: 30 May 2016

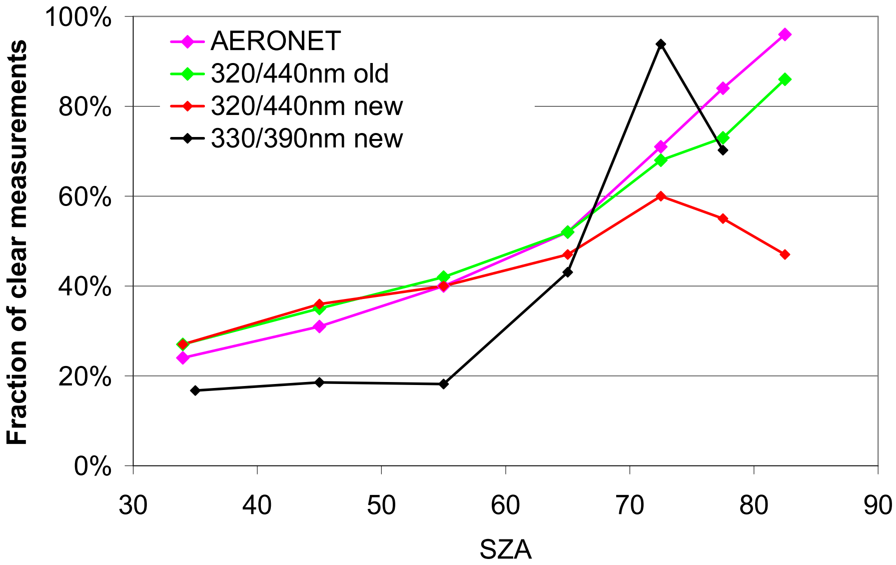

Figure 10: Dependence of the fraction of clear sky observations on SZA for MAX-DOAS and AERONET observations.

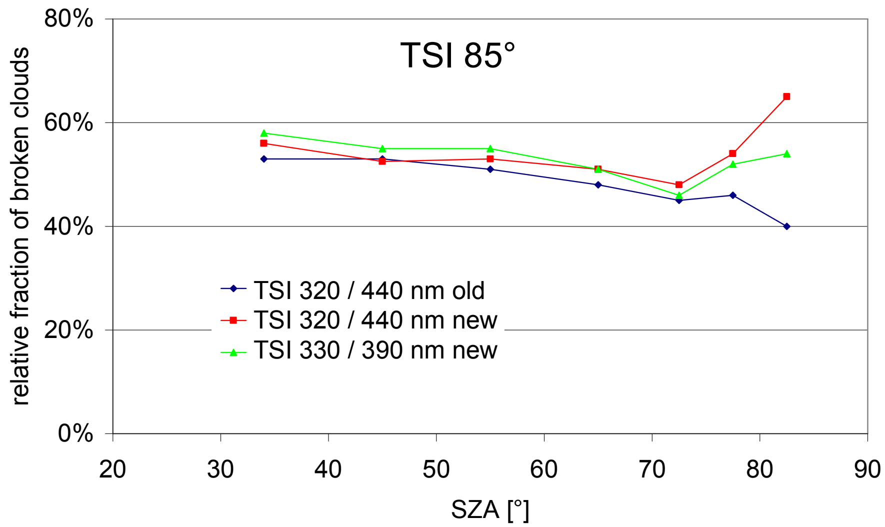

Figure 11: Fraction of measurements, for which the Temporal Smoothness Indicator (TSI, see section 4.2) for elevation angle of 85° exceeds the threshold values. Enhanced TSI indicate the presence of broken clouds.

Atmos. Meas. Tech. Discuss., doi:10.5194/amt-2016-148, 2016
Manuscript under review for journal Atmos. Meas. Tech.
Published: 30 May 2016

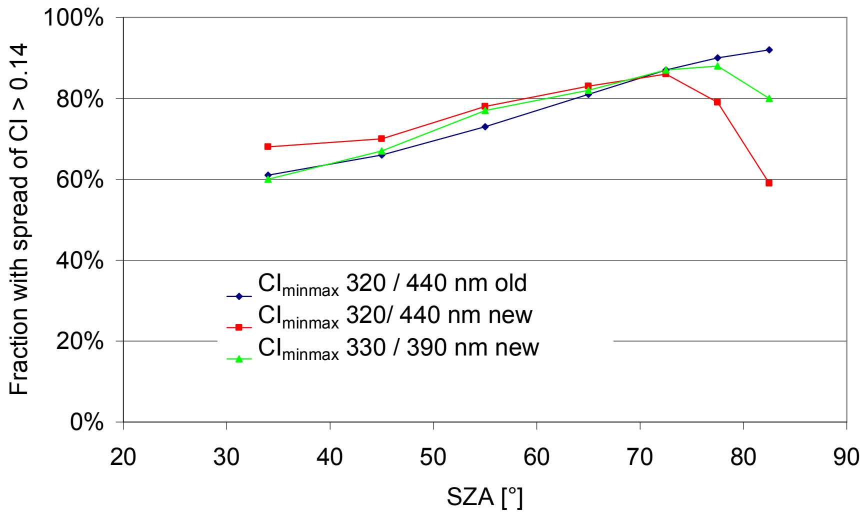

Figure 12: Relative fraction of measurements, for which the spread of the CI exceeds the threshold value of 0.14.

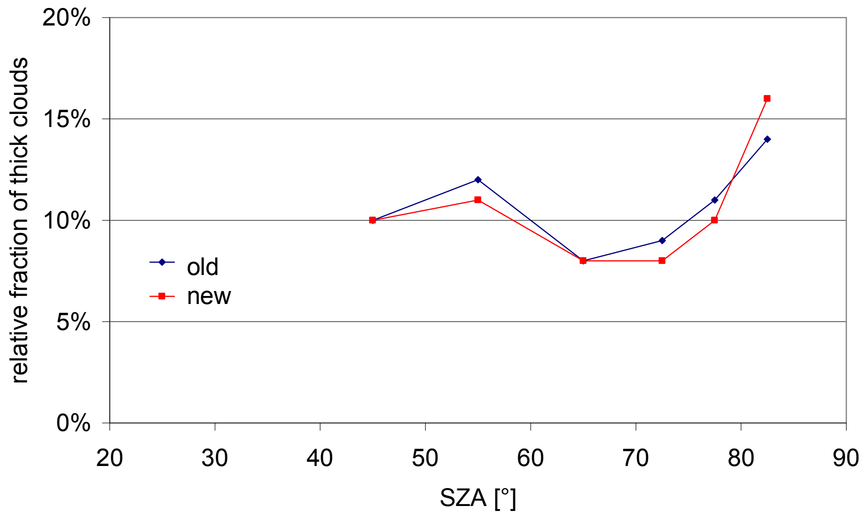

Figure 13: Fraction of measurements with O_4 AMFs > the threshold for the appearance of thick clouds.

Atmos. Meas. Tech. Discuss., doi:10.5194/amt-2016-148, 2016
Manuscript under review for journal Atmos. Meas. Tech.
Published: 30 May 2016

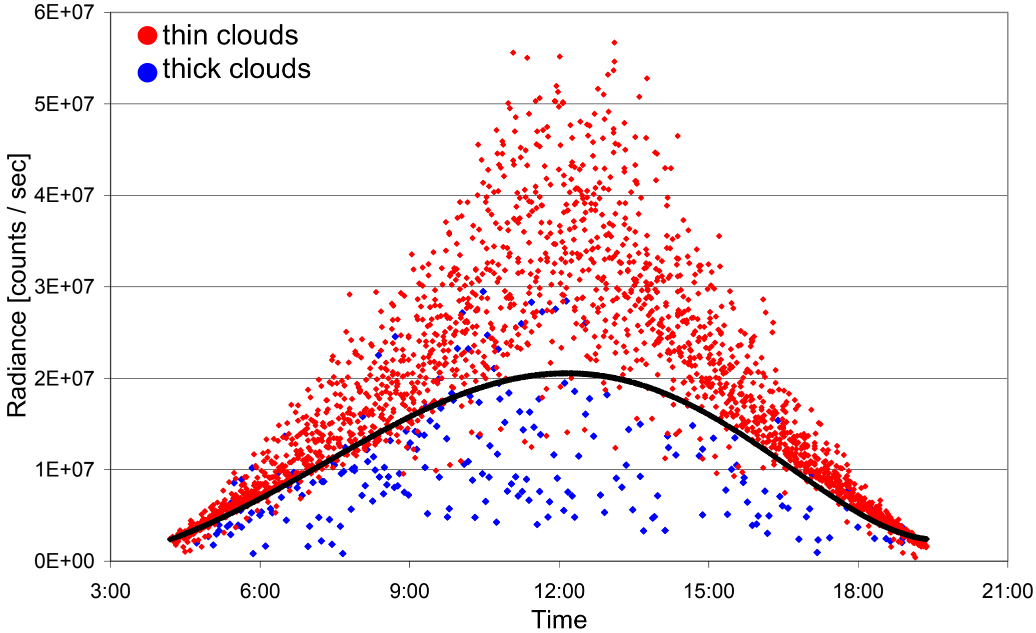

Figure 14: Measured radiance (in units of counts/sec) for near-zenith observations during the Cabauw campaign. The blue/red dots indicate measurements, which were classified as under optically thick/thin clouds, respectively, based on the calibrated O_4 absorption using the updated thresholds. The black curve represents the threshold value for the radiance used in the original version of the algorithm. The measurements are from the period 12 June to 15 July 2009.

Atmos. Meas. Tech. Discuss., doi:10.5194/amt-2016-148, 2016
Manuscript under review for journal Atmos. Meas. Tech.
Published: 30 May 2016

Atmospheric Measurement Techniques
Open Access
Discussions

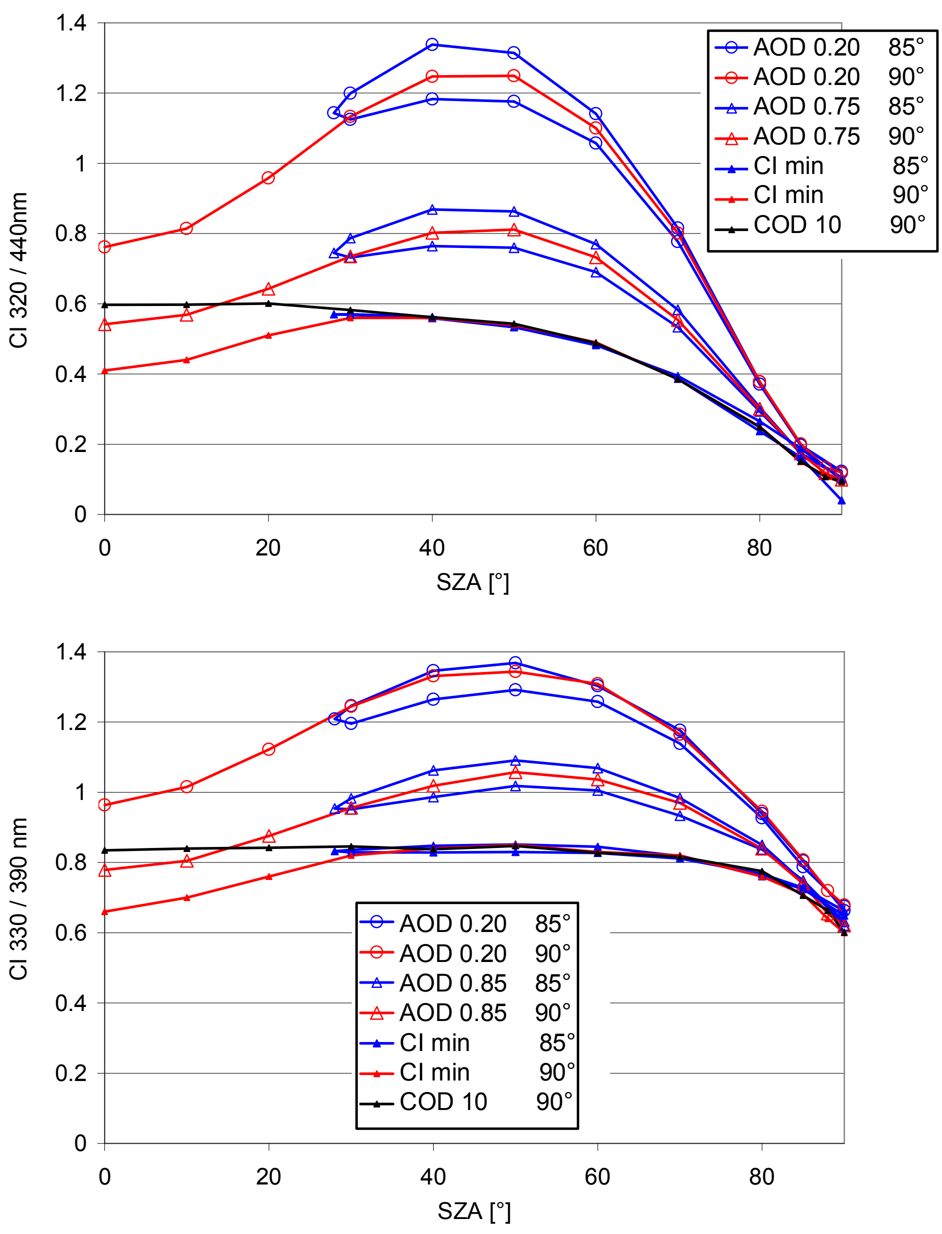

Figure 15: Comparison of simulated CI (top: $CI_{orig:}$ 320 nm / 440 nm; bottom: CI_{new}: 330 nm / 390 nm) for elevation angles of 85° (blue lines) and 90° (red lines). The different symbols represents different atmospheric scenarios. The black line represents results for a cloud optical depth of 10.

Atmos. Meas. Tech. Discuss., doi:10.5194/amt-2016-148, 2016
Manuscript under review for journal Atmos. Meas. Tech.
Published: 30 May 2016

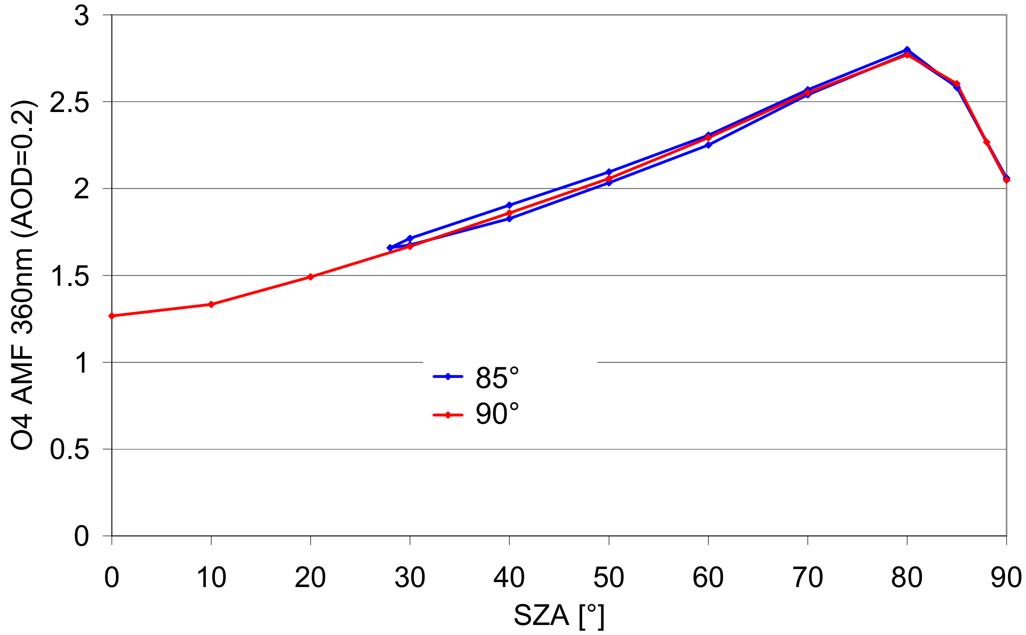

Figure 16: Comparison of the clear sky reference values of the O_4 AMF for elevation angles of 85° and 90°.

Atmos. Meas. Tech. Discuss., doi:10.5194/amt-2016-148, 2016
Manuscript under review for journal Atmos. Meas. Tech.
Published: 30 May 2016

Atmospheric Measurement Techniques Discussions

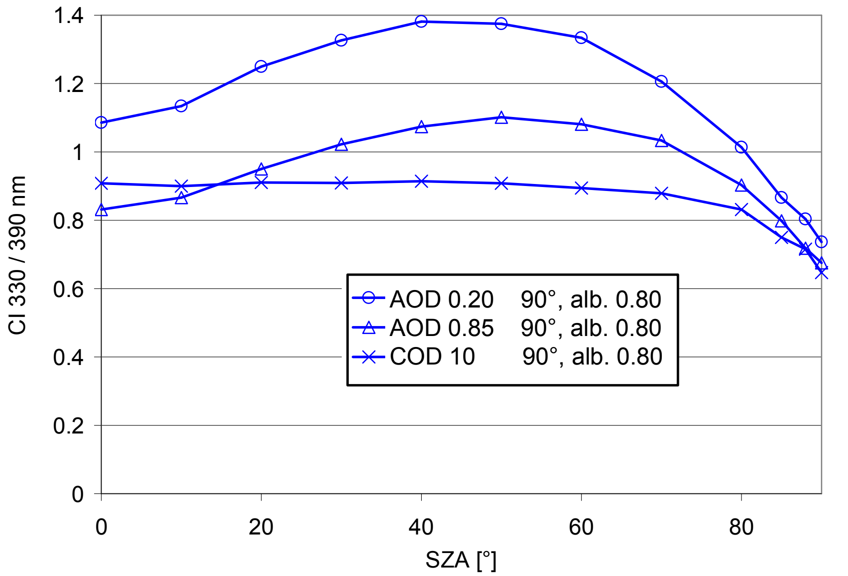

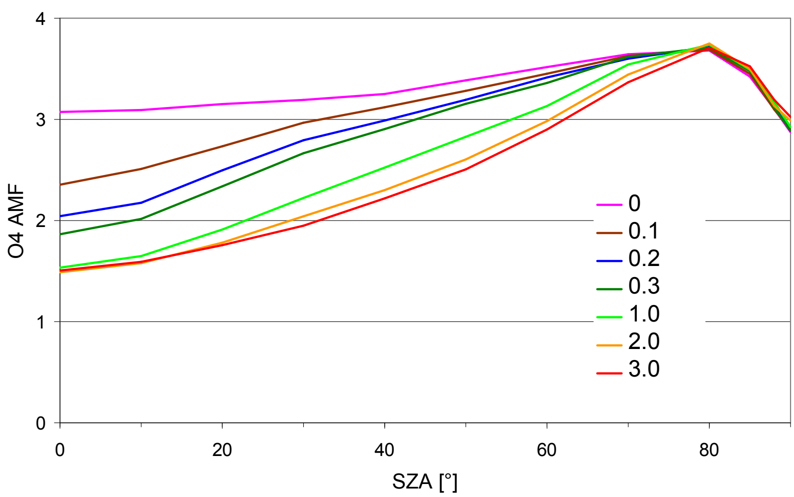

5 **Figure 17: Simlated CI (top) and O_4 AMF (bottom) for zenith direction for clear sky measurements above bright surfaces (albedo =80%). The different colours indicate results for different AOD.**

Atmos. Meas. Tech. Discuss., doi:10.5194/amt-2016-148, 2016
Manuscript under review for journal Atmos. Meas. Tech.
Published: 30 May 2016

Appendix

Table A1 Tabulated values for the SZA dependent thresholds of the different quantities

SZA	CI 320 / 440	CI 330 / 390	TSI CI 320 / 440	TSI CI 330 / 390	O_4 AMF zenith
0	0.540	0.779	7.38E-08	6.37E-08	1.27
2	0.545	0.778	7.36E-08	6.29E-08	1.28
4	0.550	0.781	7.38E-08	6.27E-08	1.30
6	0.556	0.786	7.46E-08	6.33E-08	1.31
8	0.564	0.794	7.59E-08	6.43E-08	1.32
10	0.573	0.804	7.78E-08	6.57E-08	1.34
12	0.584	0.816	8.02E-08	6.74E-08	1.36
14	0.596	0.830	8.31E-08	6.94E-08	1.38
16	0.609	0.844	8.66E-08	7.16E-08	1.41
18	0.624	0.860	9.05E-08	7.39E-08	1.44
20	0.641	0.876	9.49E-08	7.64E-08	1.48
22	0.658	0.892	9.95E-08	7.89E-08	1.51
24	0.676	0.908	1.05E-07	8.15E-08	1.55
26	0.694	0.925	1.10E-07	8.41E-08	1.59
28	0.712	0.941	1.15E-07	8.68E-08	1.63
30	0.730	0.956	1.20E-07	8.94E-08	1.67
32	0.748	0.971	1.25E-07	9.19E-08	1.72
34	0.764	0.985	1.30E-07	9.44E-08	1.76
36	0.779	0.998	1.35E-07	9.67E-08	1.79
38	0.793	1.010	1.39E-07	9.89E-08	1.83
40	0.804	1.021	1.43E-07	1.01E-07	1.87
42	0.813	1.030	1.46E-07	1.03E-07	1.90
44	0.818	1.038	1.48E-07	1.04E-07	1.94
46	0.821	1.045	1.49E-07	1.05E-07	1.98
48	0.820	1.049	1.50E-07	1.06E-07	2.01
50	0.816	1.053	1.49E-07	1.06E-07	2.05
52	0.808	1.054	1.48E-07	1.06E-07	2.09
54	0.795	1.053	1.45E-07	1.05E-07	2.13
56	0.779	1.051	1.41E-07	1.03E-07	2.18
58	0.758	1.046	1.36E-07	1.01E-07	2.22
60	0.733	1.040	1.30E-07	9.84E-08	2.28
62	0.703	1.031	1.23E-07	9.48E-08	2.33
64	0.670	1.020	1.14E-07	9.06E-08	2.39
66	0.632	1.006	1.05E-07	8.56E-08	2.45
68	0.591	0.990	9.50E-08	7.99E-08	2.52
70	0.547	0.971	8.43E-08	7.36E-08	2.58
72	0.500	0.950	7.31E-08	6.68E-08	2.64
74	0.451	0.926	6.17E-08	5.96E-08	2.69
76	0.401	0.899	5.03E-08	5.21E-08	2.73
78	0.350	0.869	3.92E-08	4.46E-08	2.75
80	0.299	0.835	2.90E-08	3.72E-08	2.75
82	0.250	0.798	1.99E-08	3.04E-08	2.72
84	0.203	0.758	1.25E-08	2.44E-08	2.64
86	0.160	0.714	7.33E-09	1.97E-08	2.51
88	0.122	0.666	5.00E-09	1.67E-08	2.31
90	0.091	0.614	6.18E-09	1.61E-08	2.03

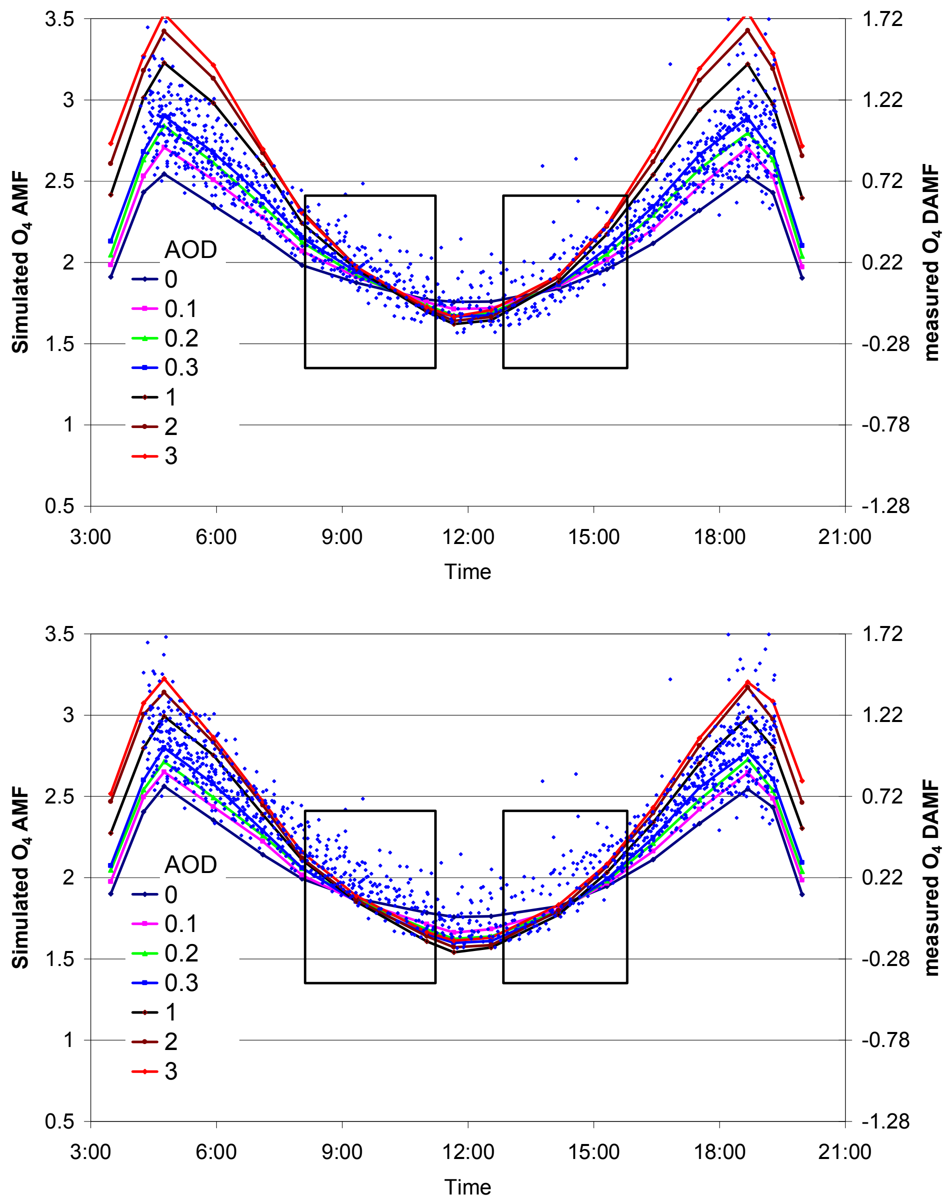

Figure A1: Comparison of measured O_4 DAMFs (only clear sky observations, right axis) with simulated O_4 AMFs (left axis) for clear sky conditions and different AOD (top: aerosol layer height of 500 m; bottom: aerosol layer height of 2000 m). The rectangles indicate the SZA ranges (30° to 50°), which are used for the calibration of the O_4 measurements. The measurements are from the period 12 June to 15 July 2009; the simulations are performed for a day (26 June 2009) in the middle of the campaign.

Atmos. Meas. Tech. Discuss., doi:10.5194/amt-2016-148, 2016
Manuscript under review for journal Atmos. Meas. Tech.
Published: 30 May 2016

Atmospheric Measurement Techniques
Discussions

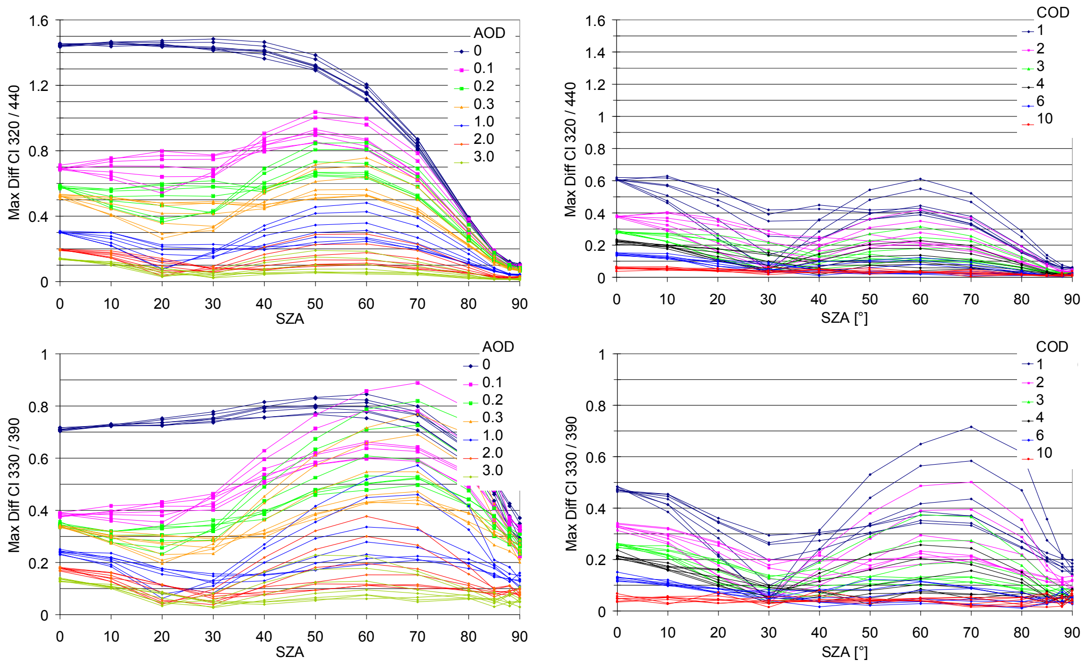

Figure A2: Spread of the CI (top: CI_{orig}: 320 nm / 440 nm; bottom: CI_{new}: 330 nm / 390 nm) between the different elevation angles for different aerosol (left) and cloud (right) scenarios. The spread is calculated as the difference between the maximum and minimum CI for a given combination of SZA and relative azimuth angle. The different lines of the same colour represent simulations for different relative azimuth angles (0°, 30°, 60°, 90°, 120°, 150°, 180°). The simulations are made assuming an elevation ange of 85° for 'zenith' view.

Atmos. Meas. Tech. Discuss., doi:10.5194/amt-2016-148, 2016
Manuscript under review for journal Atmos. Meas. Tech.
Published: 30 May 2016

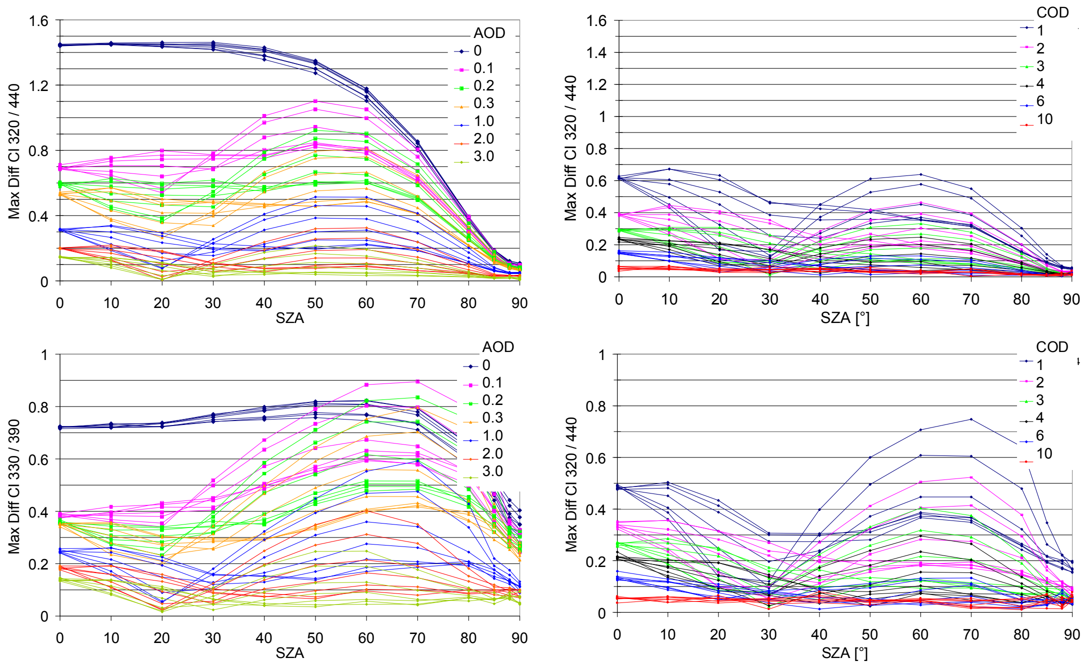

Figure A3: Same results as in Fig. A2, but for zenith observations at exactly 90° elevation.

5